Diverse roles of SERPINE1 in regulating cellular proliferation and invasion

WEI WANG[1*], PENGFEI ZHAO[2,3*], TIAN WANG[4], WEIJING WU[5], JING LI[4], QIANG HUANG[2] and JING MO[4]

[1]Department of Neurosurgery, The Second Hospital of Tianjin Medical University, Tianjin 300211, P.R. China; [2]Department of Neurosurgery, General Hospital of Tianjin Medical University, Tianjin 300052, P.R. China; [3]Department of Neurosurgery, Affiliated Hospital of Hebei University, Baoding, Hebei 071000, P.R. China; [4]Department of Pathology, Tianjin Medical University, Tianjin 300070, P.R. China; [5]Department of Biological and Pharmaceutical Engineering, School of Life Science, Shandong University, Qingdao, Shandong 266237, P.R. China

Received September 10, 2025; Accepted February 20, 2026

DOI: 10.3892/ijo.2026.5871

Abstract. Serine protease inhibitor clade E member 1 (SERPINE1) is involved in various biological processes, but its role in promoting or suppressing tumorigenesis remains controversial. The present study focused on the effects of SERPINE1 downregulation on cell proliferation and invasion across three types of tumors to elucidate the underlying mechanisms. Based on data from an analysis of The Cancer Genome Atlas dataset, high SERPINE1 levels in patients with breast cancer and low-grade glioma were associated with a poor prognosis, whereas elevated SERPINE1 expression in patients with skin cutaneous melanoma associated with improved outcomes. With respect to cell proliferation phenotypes, SERPINE1 knockdown increased xenograft growth and the proliferation of melanoma C918 cells by promoting cell cycle progression through the modulation of minichromosome maintenance complex component 3 and the activity of p53/SMAD3 regulators; conversely, SERPINE1 knockdown reduced the xenograft growth and proliferation of MDA-MB-231 breast cancer cells by decreasing the urokinase-type plasminogen activator receptor-mediated ERK/p38 activity ratio and similarly decreased proliferation in H4 glioma cells through an heat shock protein 90-alpha (HSP90α)-mediated reduction in the ERK/p38 activity ratio. Regarding invasion and metastasis, SERPINE1 knockdown consistently reduced invasion, matrix metalloproteinase (MMP) activity, and lung metastasis in both C918 and MDA-MB-231 cells but paradoxically increased invasion and MMP-1 activity in H4 cells through the HSP90α-p38-MMP-1 axis. Collectively, these findings suggested that SERPINE1 exerts diverse effects on cell proliferation and invasion through multiple regulatory mechanisms. These findings indicated that therapy targeting SERPINE1, which involves a comprehensive understanding of its diverse mechanisms of function, can increase treatment precision and reduce adverse reactions.

Correspondence to: Professor Jing Mo, Department of Pathology, Tianjin Medical University, 22 Qixiangtai Road, Heping, Tianjin 300070, P.R. China
E-mail: mojing@tmu.edu.cn

Professor Qiang Huang, Department of Neurosurgery, General Hospital of Tianjin Medical University, 154 Anshan Road, Heping, Tianjin 300052, P.R. China
E-mail: huangqiang209@163.com

*Contributed equally

Abbreviations: BRCA, breast cancer; CancerSEA, cancer single-cell state atlas; CSCs, cancer stem cells; DEGs, differentially expressed genes; ELISA, enzyme-linked immunosorbent assay; EMT, epithelial-mesenchymal transition; FBS, fetal bovine serum; FDR, false discovery rate; FPKM, fragments per kilobase of transcript per million mapped reads; GEPIA2, gene expression profiling interactive analysis 2; GFP, green fluorescent protein; GO, Gene Ontology; GSEA, gene set enrichment analysis; HR, hazard ratio; HSP90α, heat shock protein 90-alpha; HSP90AA1, heat shock protein 90 alpha family class a member 1; KEGG, Kyoto Encyclopedia of Genes And Genomes; LGG, low-grade glioma; MCM3, minichromosome maintenance complex component 3; MMP, matrix metalloproteinases; PLAUR, plasminogen activator, urokinase receptor; RNA-seq, RNA sequencing; SA-β-gal, sa-β-galactosidase; SERPINE1, serine protease inhibitor clade e member 1; SKCM, skin cutaneous melanoma; TCGA, the cancer genome atlas; uPA, urokinase-type plasminogen activator; uPAR, urokinase-type plasminogen activator receptor; WGCNA, weighted correlation network analysis

Key words: heat shock protein 90α, invasion, matrix metalloproteinase-1, proliferation, serine protease inhibitor clade E member 1

Introduction

Understanding the multifaceted roles of various factors in tumor development and progression is central to understanding cancer biology. For instance, cancer driver genes, which were initially identified in specific tumor types, may exert different effects on other tumor types (1). Cellular regulators, bioactive molecules, and transcription factors also display distinct activities across different cell types (2-4). Similarly, the molecular classification of tumors is largely determined by their tissue of origin (5-7). Therefore, elucidating these diverse regulatory

mechanisms is essential for developing more effective, personalized treatments.

Serine protease inhibitor clade E member 1 (SERPINE1), also known as plasminogen activator inhibitor-1, is also a multifaceted molecule that plays significant roles in various biological processes (8). It is particularly involved in the intricate interplay between tumor progression and the modulation of immune responses through mechanisms such as promoting vascular formation via interactions with endothelial cells, regulating extracellular matrix remodeling and cellular motility, protecting tumor cells from programmed cell death, and influencing inflammatory responses and immune cell functions (9). Paradoxically, although SERPINE1 functions as a plasminogen activator inhibitor and should theoretically exert tumor-suppressive effects, high SERPINE1 expression is generally associated with tumor aggressiveness, tumor metastasis and a poor prognosis (10). Given its protumorigenic role, SERPINE1 is a pivotal target for cancer treatment. However, three major challenges complicate its clinical development: First, concentration-dependent biphasic effects, in which moderate SERPINE1 levels may inhibit tumor growth while excessive levels promote progression; second, context-dependent functionality, as the effects of SERPINE1 are modulated by the tumor microenvironment and can be opposite in different cell types and tissue contexts; and third, pathway pleiotropy, with SERPINE1 exerting diverse biological effects through multiple signaling pathways, including the urokinase-type plasminogen activator (uPA)/urokinase-type plasminogen activator receptor (uPAR) system, integrin pathway, and transforming growth factor-beta (TGF-β) pathway (11).

Numerous studies have demonstrated that SERPINE1 has antiapoptotic and proproliferative effects (12-18). For instance, SERPINE1 inhibits drug-induced apoptosis in human promyelocytic leukemia cell lines and prostate cancer cell lines by activating the NF-κB pathway (12). SERPINE1 facilitates tumor growth in esophageal squamous cell carcinoma through the activation of AKT and ERK1/2 signaling (13). SERPINE1 exerts its tumor-promoting effects on bladder and cervical cancer cells by promoting G_1 phase progression via the upregulation of cyclin D3/CDK4/6 and cyclin E/CDK2 complexes (14). SERPINE1 promotes neuronal survival via low-density lipoprotein receptor-related protein 1 by activating the PI3K/AKT pathway and inhibiting the JNK/NF-κB pathway (15). However, the anti-proliferative activity of SERPINE1 has been observed in certain contexts. For instance, high expression of SERPINE1 in human renal epithelial cells leads to proliferative defects, which are mediated by a loss of klotho expression, the consequent upregulation of p53, and increased phosphorylation of SMAD3 (16). The suppression of SERPINE1 allows ageing fibroblasts to bypass senescence through the p53-p21-Rb pathway (17,18).

SERPINE1 also exerts stimulatory, inhibitory, and neutral effects on invasion/metastasis. Its proinvasive/metastatic effects are described hereafter. SERPINE1 facilitates tumor cell migration by inducing detachment from vitronectin and promoting redirected migration to fibronectin (19). SERPINE1 enables invasion by inhibiting uPAR-bound uPA to protect the integrity of matrix proteins essential for adhesion and migration (20). SERPINE1 facilitates glioblastoma spread by altering adhesion and reprogramming transcription (21). Through upregulation of matrix metalloproteinase-13 (MMP-13) expression and secretion, SERPINE1 increases invasion and facilitates pulmonary metastasis in osteosarcoma (22). The SERPINE1 and CCL5 signaling pathways in endothelial cells cooperate to potentiate the metastatic spread of triple-negative breast cancer cells that have undergone the epithelial-mesenchymal transition (EMT) (23). In non-small cell lung cancer (NSCLC), a SERPINE1/PIAS3/Stat3/miR-34a positive feedback loop enhances EMT-mediated metastasis (24). Its anti-invasive/metastatic effects include the following: Overexpression of SERPINE1 suppresses the hepatic metastasis of pancreatic cancer and inhibits the invasiveness of glioma cells (25,26); SERPINE1, upregulated by TGF-β, suppresses the migration and invasion of melanoma cells by inhibiting the plasminogen activation system (27); the increased expression of SERPINE1 in malignant prostate cells results in the acquisition of a less invasive phenotype (28); and SERPINE1 contributes to fibrous adhesion in injured flexor tendons by reducing MMP activity (29).

SERPINE1 modulates cell proliferation and invasion through complex regulatory networks. Additional mechanisms potentially contribute to these processes, whereas previously identified mechanisms may exhibit context-dependent functional variations. The present study aims to elucidate potentially novel mechanisms underlying the role of SERPINE1 in regulating cellular proliferation and invasion, providing fundamental support for the development of SERPINE1-directed antitumor interventions.

Materials and methods

Gene expression profiling interactive analysis 2 (GEPIA2) and cancer single-cell state atlas (CancerSEA). Kaplan-Meier survival curves were generated using the GEPIA2 database (30) (http://gepia2.cancer-pku.cn/), with expression data (in transcripts per million; TPM) and clinical survival data sourced from The Cancer Genome Atlas (TCGA) Research Network (accessed July 11, 2016; version: Legacy, GRCh37 (hg19); https://www.cancer.gov/about-nci/organization/ccg/research/structural-genomics/tcga). For a given type of cancer, the cohort was split into two groups based on SERPINE1 expression using a quartile-based cutoff: Tumors with expression levels at or above the 75th percentile were classified as the 'High expression' group, and those at or below the 25th percentile as the 'Low expression' group; a method that minimizes outlier effects. The platform plotted the Kaplan-Meier estimator for each group and the statistical significance of the difference between survival curves is computed using the log-rank (Mantel-Cox) test, outputting the hazard ratio (HR) with its 95% confidence interval and the log-rank P-value. This specific pan-cancer comparison was generated using the 'Survival Map' function in GEPIA2. For breast cancer (BRCA), there are 1,085 tumor samples and 291 normal samples; for low-grade glioma (LGG), 518 tumor samples and 207 normal samples; and for skin cutaneous melanoma (SKCM), 461 tumor samples and 558 normal samples.

To decode the functional relevance of SERPINE1 at single-cell resolution, the present study used the CancerSEA database (31) (http://biocc.hrbmu.edu.cn/CancerSEA), which employs an established pipeline involving 14 manually curated

cancer-relevant functional states represented by specific gene signatures, quantifies the activity of each state in individual cancer cells (from 41,900 cells across 25 types of cancers) using Gene Set Variation Analysis (GSVA), and evaluates the relationship between SERPINE1 expression and each functional state's GSVA score via Spearman's rank correlation coefficient, with significant associations defined as absolute Spearman's $\rho>0.3$ and Benjamini-Hochberg adjusted P-value [false discovery rate (FDR)]<0.05; these significant correlation coefficients were visualized in a heatmap.

Cell lines and cell culture. The human breast cancer cell line MDA-MB-231 (abbreviated as 231), glioma cell line H4, melanoma cell line C918 and 293T cells were obtained from the Cell Resource Center (Peking Union Medical College, Beijing, China). Cell lines were authenticated by short tandem repeat testing and mycoplasma contamination was absent. Cells were cultured in Dulbecco's modified Eagle's medium (cat. no. KGL1206-500; Jiangsu KeyGen Biotech Co., Ltd.) supplemented with 10% fetal bovine serum (FBS; cat. no. 164210, Pricella; Elabscience Bionovation Inc.) and 1% penicillin/streptomycin and maintained at 37˚C with 5% CO_2 in a humidified incubator.

Cell transfection. A third-generation lentiviral system was used to establish stable knockdown or overexpression cell lines. All lentiviral constructs were purchased from Genechem Co., Ltd. (Shanghai, China). Lentiviruses were produced using the Lenti-Pac HIV Expression Packaging Kit (cat. no. LT001; GeneCopoeia, Inc.) according to the manufacturer's instructions. Briefly, 293T cells were co-transfected with 2.5 μg of lentiviral expression plasmid and 2.5 μg of Lenti-Pac mixed packaging plasmid (containing packaging and envelope components) at 37˚C with 5% CO_2. At 48 h post-transfection, viral supernatants were collected, centrifuged, and filtered. Target cells were infected at a multiplicity of infection (MOI) of 3. After 14 days of selection with puromycin (4 μg/ml) (cat. no. HY-B1743; MedChemExpress) or G418 (800 μg/ml) (cat. no. HY-17561; MedChemExpress), stably transduced cells were maintained in medium containing the same antibiotic concentrations and used for subsequent experiments. This procedure was applied in experiments involving SERPINE1 knockdown, SERPINE1 rescue, and uPAR overexpression.

For SERPINE1 knockdown, two lentiviral constructs were utilized: an shRNA targeting SERPINE1 (abbreviated as shSE1) and a scrambled control shRNA (abbreviated as shc). The two shSE1 constructs targeted two sequences: 5'-AGA CCAACAAGTTCAACTATA-3' (Target 1) and 5'-TCTCTG CCCTCACCAACATTC-3' (Target 2). The scrambled control shc targeted the sequence 5'-TTCTCCGAACGTGTCACGT-3'. These constructs were used to transduce MDA-MB-231, C918, and H4 cells. Stable cell lines were selected with puromycin (4 μg/ml) for 14 days before being used in subsequent experiments.

A functional rescue experiment was performed to confirm that the observed phenotypes were specifically caused by SERPINE1 knockdown rather than by off-target effects. An shRNA-resistant SERPINE1 cDNA construct was generated by introducing six synonymous mutations into the 21-nt region (TCTCTGCCCTCACCAACATTC) targeted by the shRNA, thereby preserving the native amino acid sequence while preventing shRNA binding. The mutated DNA sequence (5'-TCCCTGCCATCGACTACATTC-3') was subsequently cloned and inserted into a lentiviral expression vector. This rescue lentivirus, along with a control empty vector (abbreviated as vec), were used to infect stable SERPINE1-knockdown cells (shSE1). The resulting cell lines were designated shSE1 + SE1 (rescued) and shSE1 + vec (control). Stable cell lines were selected with G418 (800 μg/ml) for 14 days before being used in subsequent experiments.

For uPAR overexpression, 231-shSE1 cells were infected with a lentivirus containing plasminogen activator, urokinase receptor (PLAUR) cDNA (abbreviated as ex-PLAUR) or the corresponding empty vector control (abbreviated as vec). Stable cell lines were selected with G418 (800 μg/ml) for 14 days before being used in subsequent experiments.

Small RNA interference (RNAi) transfection. For RNA interference targeting HSP90α (HSP90AA1), H4-shSE1 cells were seeded into 6-well plates and grown to 70-80% confluence. Transfection was performed using Lipofectamine® 2000 (Invitrogen; Thermo Fisher Scientific, Inc.) and siRNA Set A (three siRNA pairs targeting human HSP90AA1(si-HSP90AA1) and a negative control (siNC; cat. no. HY-RS06415; MedChemExpress) according to each manufacturer's protocol.

The siHSP90AA1 construct targeted three sequences: 5'-GTTATCCTACACCTGAAAGAA-3' (Target 1), 5'-AGC TGCATATTAACCTTATAC-3' (Target 2), and 5'-TACTTG GAGGAACGAAGA ATA-3' (Target 3). The negative control siRNA (siNC) targeted the sequence 5'-AATTCTCCGAAC GTGTCACGT-3'.

Enzyme-linked immunosorbent assay (ELISA). The concentration of SERPINE1 in the cell culture supernatant was measured using a human SERPINE1 ELISA Kit (cat. no. EH0538; Wuhan Fine Biotech Co., Ltd.). When the cells reached ~80% confluence, the culture medium was replaced with serum-free medium. After 24 h, the conditioned medium was collected and assayed strictly according to the manufacturer's protocol. The experiment was performed with three replicates in each group. The absorbance was read using a BioTek Synergy Mx microplate reader (Agilent Technologies, Inc.).

Western blotting. Transfected cells were harvested and lysed using RIPA buffer (cat. no. R0020; Beijing Solarbio Science & Technology Co., Ltd.) supplemented with 1 mM PMSF (cat. no. HY-B0496MedChemExpress), 10 mM DTT (cat. no. HY-15917MedChemExpress), and 10 μM protein kinase inhibitor (cat. no. P1006; Beyotime Biotechnology) on ice for 30 min. Equal amounts of protein (20 μg, quantified by BCA (cat. no. PC0020; Beijing Solarbio Science & Technology Co., Ltd.) were separated by SDS-PAGE (4-20% gradient gel; cat. no. ET15420L; ACE Biotechnology) and transferred to 0.2 μm pore size PVDF membranes (cat. no. ISEQ00010; Merck Sharp & Dohme-Hoddesdon). Following the blocking of nonspecific binding sites using 5% skimmed milk (cat. no. P0216; Beyotime Biotechnology) or bovine serum albumin (cat. no. NGP0028A; Beyotime Biotechnology) for

1 h at room temperature, the membranes were incubated with primary antibodies (incubation overnight at 4˚C) against SERPINE1 (cat. no. 13801-1-AP; Proteintech Group, Inc), GAPDH (cat. no. sc-25778; Santa Cruz Biotechnology, Inc.), MCM3 (cat. no. PA5-79646; Thermo Fisher Scientific, Inc.), phosphorylated (p-)MCM3 (Ser112; cat. no. TA2362; Abmart Pharmaceutical Technology Co., Ltd.), ERK (cat. no. sc-514302; Santa Cruz Biotechnology, Inc.), uPAR (cat. no. ab10379; Abcam), Histone H3 (cat. no. 4499), p-p53 (Ser15; cat. no. 9284), p53 (cat. no. 2524), p-SMAD3 (Ser423/425; cat. no. 9520), SMAD3 (cat. no. 9523), p-Rb (Ser807/811; cat. no. 8516), Rb (cat. no. 9309), CyclinD1 (cat. no. 55506), CyclinE1 (cat. no. 20808), p21 (cat. no. 2947), p-p38 (cat. no. 4511), p38 (cat. no. 8690), p-ERK (cat. no. 4370), p-JNK (cat. no. 9255), JNK (cat. no. 9252), p-AKT (Ser473; cat. no. 4060), AKT (cat. no. 9272), HSP90α (cat. no. 4877) and MMP-1 (cat. no. 54376) were from Cell Signaling Technology, Inc.) and subsequently incubated with the corresponding secondary antibodies (dilution 1:4,000) for 2 h at room temperature. The secondary antibodies used were horseradish peroxidase (HRP)-conjugated goat anti-rabbit (cat. no. ZB-2301; Beijing Zhongshan Jinqiao Biotechnology Co., Ltd.) and HRP-conjugated goat anti-mouse (cat. no. ZB-2305; Beijing Zhongshan Jinqiao Biotechnology Co., Ltd.). Chemiluminescence was detected using WesternBright ECL HRP substrate (cat. no. R-03031-D2; Advansta Inc.). Bands were visualized using the C-DiGit Blot Scanner (LI-COR Biosciences), and a densitometric analysis was performed using ImageJ software (version: 1.52a) (National Institutes of Health). Three independent replicates were performed for each experimental condition.

Clonogenic assays. A colony formation assay was performed to evaluate clonogenic survival by seeding single-cell suspensions at $1x10^3$ cells/well in 6-well plates. After 14 days, the colonies were fixed with 100% methanol for 10 min at room temperature. Following fixation, colonies were stained with 0.1% crystal violet solution for 30 min at room temperature. Colonies were defined as clusters containing ≥50 cells or visible colonies measuring >0.1 mm in diameter. The colony-forming efficiency was calculated as follows: (number of colonies formed/number of cells seeded) x100%. Three replicates were performed for each group.

Tumorigenicity. Subcutaneous xenograft and lung metastasis models were established to compare tumor growth and metastasis between the SERPINE1 knockdown (shSE1) and control (shc) groups of MDA-MB-231 and C918 cells *in vivo*. A total of 44 male BALB/c nu/nu mice [SiPeiFu (Beijing) Biotechnology Co., Ltd.] were used in this study. For the subcutaneous xenograft model, 20 mice (4 groups, n=5 per group) were used. For the lung metastasis model, 24 mice (4 groups, n=6 per group) were used. The mice were either 4 weeks of age, weighing 17-19 g (subcutaneous xenograft model), or 6 weeks of age, weighing 20-22 g (lung metastasis model), at the start of the experiments. The animals were housed under specific pathogen-free (SPF) conditions at a controlled temperature (22±1˚C) and humidity (40-60%), with a 12 h light/dark cycle, and provided with sterilized food and water *ad libitum*.

Humane endpoints were established to minimize animal suffering and were strictly monitored throughout the study. Mice were euthanized if any of the following criteria were met: i) Tumor volume >1,500 mm^3; ii) body weight loss exceeded 15% of initial weight; iii) signs of severe lethargy, hunched posture, or inability to access food or water; iv) ulceration or necrosis of tumor tissue; v) significant respiratory distress or impaired mobility. All endpoints were monitored by trained personnel, and no animals reached the predetermined humane endpoint criteria during this study.

For the subcutaneous xenograft model, four-week-old mice were subcutaneously injected in the axillary region with $5x10^6$ cells (231-shc, 231-shSE1, C918-shc, or C918-shSE1) in 100 μl of PBS (n=5) to evaluate tumor cell growth. Subcutaneous tumors were measured using calipers every three days, and the tumor volume was calculated using the formula: Volume (mm^3)=0.5 x length x $(width)^2$. Tumors were excised and weighed after the mice were sacrificed by cervical dislocation. The maximum diameter of the excised tumors ranged from 5 to 10 mm. The maximum volume of the excised tumors did not exceed 1,500 mm^3.

For the lung metastasis model, six-week-old mice were injected via the tail vein with $1x10^4$ cells (231-shc, 231-shSE1, C918-shc, or C918-shSE1) in 50 μl of PBS (n=6) to analyze lung metastatic colonization. Lung metastases were assessed four weeks later by performing a gross examination, hematoxylin and eosin (H&E) and green fluorescent protein (GFP) staining.

Regarding the different sample sizes (n), the variation in mouse numbers per group between the subcutaneous tumorigenicity (n=5) and hematogenous metastasis (n=6) experiments arises from a sample size adjustment that accounts for the anticipated technical success rates of each model. The sample size for each experiment was initially calculated by power analysis (α=0.05; power=80%; two-sided t-test; effect size=3.5), yielding a baseline requirement of n=4 per group, which was then increased to n=5 for the tumorigenicity assay to account for an expected tumor formation rate of ~80% for the MDA-MB-231 and C918 cell lines, and to n=6 for the metastasis assay to accommodate an expected detectable metastasis formation rate of ~70%. This adjustment was made to ensure an adequate final number of evaluable animals per group.

All the experimental protocols were performed in accordance with the guidelines and regulations of the Institutional Animal Care and Use Committee at Tianjin Medical University (approval no. TMUaMEC 2022045). All methods are reported in accordance with the ARRIVE guidelines.

H&E staining and immunohistochemical staining. For histological analysis, xenograft tumor tissues were harvested, fixed overnight in 10% neutral-buffered formalin at room temperature. Following fixation, tissues were processed through a graded ethanol series (70, 80, 95 and 100% ethanol, 1 h each), cleared in xylene (2 changes, 1 h each), and embedded in paraffin at 60˚C. The paraffin-embedded tissues were sectioned at 5 μm thickness.

For H&E staining, sections were deparaffinized in xylene (2x15 min) and rehydrated through a graded ethanol series (100, 95, 80, 70% ethanol, 5 min each) to distilled water. Hematoxylin staining was performed at room temperature for

3-5 min, followed by rinsing in running tap water for 1 min and 1% acid alcohol differentiation solution for 30 sec. After rinsing in running tap water for 1 min, sections were then counterstained with eosin Y at room temperature for 2-3 min. After staining, sections were dehydrated through graded ethanol (70, 80, 95 and 100% ethanol, 1 min each), cleared in xylene (2x5 min), and mounted with coverslips using mounting with neutral resin.

For immunostaining, slides were deparaffinized, rehydrated through a graded alcohol series, and subjected to antigen retrieval in citrate buffer using a high-pressure cooker for 15 min. Subsequently, sections were treated with 3% H_2O_2 for 10 min, washed with PBS, and blocked with 5% normal goat serum (cat. no. ZLI-9056; ZSGB-BIO) for 1 h at room temperature. Following blocking, sections were incubated with primary antibodies overnight at 4˚C. Primary antibodies used were: Anti-GFP (cat. no. 2956; Cell Signaling Technology, Inc.) at 1:100 dilution, anti-p-MCM3 (Ser112; cat. no. TA2362; Abmart Pharmaceutical Technology Co., Ltd.) at 1:300 dilution and anti-MCM3 (cat. no. PA5-79646; Thermo Fisher Scientific, Inc.) at 1:500 dilution. Antigen-antibody binding was detected using a HRP-conjugated goat anti-rabbit secondary antibody (ready-to-use solution, cat. no. AFIHC003; Aifang Biological) for 1 h at room temperature. Antigen-antibody binding was visualized using DAB chromogen solution (ready-to-use solution, cat. no. AFZD002; Aifang Biological). Sections were counterstained with hematoxylin at room temperature, dehydrated, and mounted with neutral resin. Images were captured using a light microscope (80i; Nikon Corporation).

The numbers of tissue samples used for H&E and immunohistochemical staining were n=5 for subcutaneous transplanted tumors and n=6 for pulmonary metastases.

RNA sequencing (RNA-seq) and bioinformatics analysis. For RNA-seq, RNA was extracted from cells transduced with shSE1 and shc using Trizol reagent (cat. no. R0016; Beyotime Biotechnology). RNA-seq was performed using one biological replicate per group. The total RNA quantity and purity were analyzed using an RNA 6000 Nano LabChip Kit (cat. no. 5067-1511; Agilent Technologies, Inc.) on a Bioanalyzer 2100 system (Agilent Technologies, Inc.). High-quality RNA samples with a RNA Integrity Number (RIN) >7.0 were used to construct a sequencing library. mRNA was purified from total RNA (5 μg) using Dynabeads Oligo (dT; Thermo Fisher Scientific, Inc.) with two rounds of purification. Following purification, the mRNA was fragmented into short fragments using divalent cations under elevated temperature [Magnesium RNA Fragmentation Module (cat. no. e6150; New England BioLabs, Inc.) under 94˚C 5-7 min]. Then the cleaved RNA fragments were reverse-transcribed to create the cDNA by SuperScript II Reverse Transcriptase (cat. no. 1896649; Invitrogen; Thermo Fisher Scientific, Inc.), which were next used to synthesized U-labeled second-stranded DNAs with *E. coli* DNA polymerase I (cat. no. m0209; New England BioLabs, Inc.), RNase H (cat. no. m0297; New England BioLabs, Inc.) and dUTP Solution (cat. no. R0133; Thermo Fisher Scientific, Inc.). An A-base was then added to the blunt ends of each strand, preparing them for ligation to the indexed adapters. Each adapter contained a T-base overhang for ligating the adapter to the A-tailed fragmented DNA. Dual-index adapters were ligated to the fragments, and size selection was performed with AMPureXP beads. After the heat-labile UDG enzyme (cat. no. m0280; New England BioLabs, Inc.) treatment of the U-labeled second-stranded DNAs, the ligated products were amplified with PCR by the following conditions: initial denaturation at 95˚C for 3 min; 8 cycles of denaturation at 98˚C for 15 sec, annealing at 60˚C for 15 sec, and extension at 72˚C for 30 sec; and then final extension at 72˚C for 5 min. The average insert size for the final cDNA libraries were 300±50 bp. Final library concentrations were determined using Qubit dsDNA HS Assay Kit (Thermo Fisher Scientific, Inc.) and diluted to 2 nM in TE buffer. Libraries were pooled equimolarly and subjected to 2x150 bp paired-end sequencing (PE150) on the Illumina NovaSeq 6000 platform (Illumina Inc.). The reads were further filtered using Cutadapt (https://cutadapt.readthedocs.io/en/stable/, version cutadapt-1.9) to obtain high-quality reads. Reads from all the samples were aligned to the *Homo sapiens* reference genome using HISAT2 (https://daehwankimlab.github.io/hisat2/, version hisat2-2.2.1). StringTie (http://ccb.jhu.edu/software/stringtie/, version stringtie-2.1.6) and ballgown (http://www.bioconductor.org/packages/release/bioc/html/ballgown.html) were used to estimate the expression levels of all transcripts by calculating fragments per kilobase of transcript per million mapped reads (FPKM) values.

An analysis of differentially expressed genes (DEGs) between two comparative groups (shSE1 vs. shc) was performed using edgeR (version 3.38.4, https://bioconductor.org/packages/release/bioc/html/edgeR.html) with the glmQLFit and glmQLFTest functions. Genes whose FDR was <0.05 and whose absolute fold change was ≥2 were considered DEGs.

Gene Ontology (GO) enrichment analysis and Kyoto Encyclopedia of Genes and Genomes (KEGG) pathway enrichment analysis (32) were performed using clusterProfiler (version 4.4.4, https://bioconductor.org/packages/release/bioc/html/clusterProfiler.html) with the enrichGO and enrichKEGG functions, respectively. Gene set enrichment analysis (GSEA) was conducted using the clusterProfiler GSEA function with the Molecular Signatures Database (MSigDB) hallmark gene sets. Weighted correlation network analysis (WGCNA) was performed using the OmicShare platform (https://www.omicshare.com/tools) to identify co-expression modules.

Detection of cell cycle, cell cycle-related proteins and exogenous TGF-β1 treatment. C918-shc and C918-shSE1 cells were stained with propidium iodide in the presence of 100 μg/ml RNase A (cat. no. E-CK-A351; Elabscience; Elabscience Bionovation Inc.) to examine the distribution of cells in different phases of the cell cycle. The fluorescence was detected and analyzed using a BD FACSVerse flow cytometer (BD Biosciences). The expression of 89 human cell cycle-related proteins was assessed using a label-based antibody array (cat. no. AAH-BLG-CYC-4, RayBiotech, Inc.) according to the manufacturer's protocol. Each protein on the array was detected using four biological replicates.

The cells were treated with 0.5 ng/ml recombinant human TGF-β1 (cat. no. HY-P70543; MedChemExpress) or vehicle (4 mM HCl supplemented with 0.1% BSA) for 24 h

to determine how exogenous TGF-β1 alters the expression of cell cycle-related proteins in C918-shSE1 cells, with three replicates per group. After treatment, the cells were harvested and were subjected to western blotting analysis and cell cycle detection.

Induction and quantitation of anoikis. Poly-hydroxyethyl methacrylate (cat. no. P3932; MilliporeSigma) was dissolved in ethanol at 100 mg/ml and coated on 6-well plates. Cells were plated on these wells and incubated for 72 h to induce anoikis. Subsequently, suspended cells were harvested, and anoikis was quantified using an Annexin V-APC/DAPI apoptosis detection kit (cat. no. E-CK-A258; Elabscience Bionovation Inc.) according to the manufacturer's instructions. Briefly, cells were washed twice with cold PBS and resuspended in 100 μl binding buffer. Annexin V-APC (5 μl) and DAPI (5 μl) were added to each sample and incubated for 15 min at room temperature protected from light. After incubation, 400 μl binding buffer was added to each tube, and samples were analyzed immediately by flow cytometry using a BD FACSVerse instrument (BD Biosciences). The total apoptotic rate was calculated as the percentage of Annexin V-positive cells (including both early apoptotic (Annexin $V^+/DAPI^-$) and late apoptotic/necrotic (Annexin $V^+/DAPI^+$) cells). Data were analyzed using FlowJo software (version 10.6.2; BD Biosciences). Three replicates were performed for each group.

Migration and invasion assays. To detect the effects of SERPINE1 downregulation on migration and invasion in 231, H4, and C918 cells, Transwell assays were performed with SERPINE1 downregulation (shSE1) and control (shc) groups. The number of migrated cells was quantified from three randomly selected microscopic fields per membrane. Images were captured using a light microscope (80i; Nikon Corporation).

For the Transwell migration assays, 8-μm Transwell chambers (cat. no. 725321; Wuhan NEST Biotechnology Co., Ltd.) were used. Serum-starved cells ($1x10^4$ cells/well) were plated in the upper chambers with 100 μl of FBS-free medium, and 400 μl of 10% FBS medium was added to the lower chambers. The cells that migrated through the membrane were counted and images captured after 24 h.

For the Transwell invasion assays, $4x10^4$ cells in 100 μl of FBS-free medium were plated in the top chamber precoated with Matrigel (cat. no. 0827045; Xiamen Mogengel Biotechnology Co., Ltd.) or neutralized Collagen Type I (cat. no. 08-115; MilliporeSigma). Matrigel was kept chilled on ice throughout all preparation steps. First, frozen Matrigel was thawed overnight at 4˚C in a refrigerator. Then, the Matrigel was diluted with chilled serum-free medium at a ratio of 1:2 (Matrigel:medium). Next, 100 μl of the diluted Matrigel was added to the top chamber of each Transwell insert. Finally, the plates were placed in a humidified incubator at 37˚C for 60 min to allow the Matrigel to form a gel. Collagen I solutions were neutralized on ice with 0.1 N NaOH and diluted with serum-free medium to a final concentration of 2.1 mg/ml. Then, 100 μl of the diluted collagen solution was added to the top chamber of each Transwell insert. At 48 h post-seeding, images were taken of the cells that had invaded the Matrigel or Collagen I. For the aforementioned migration and invasion assays, each group was performed in triplicate.

Analysis of the MMP array. MMPs and their inhibitors, tissue inhibitors of metal proteases (TIMPs), were evaluated using a Human MMP Array (cat. no. QAH-MMP-1-1; RayBiotech, Inc.) with tenfold concentrated cell supernatants and the assays were conducted in four replicates.

Fluorescence-based MMP activity assays. The activities of MMP-1 and MMP-13 in cell lysates were measured using fluorescence kits (cat. nos. GMS50069.1.v.A for MMP-1 and GMS50076.1.v.A for MMP-13; GENMED) according to the manufacturer's protocol. The fluorescence intensity was recorded every 5 min for 30 min at 37˚C using a Bio-Tek SynergyMx plate reader (excitation/emission wavelengths: 490/525 nm; Agilent Technologies, Inc.). The experiment was performed with three replicates in each group.

Identification of gene coexpression modules. WGCNA was employed to identify modules in BRCA, LGG, and SKCM tissues that were markedly associated with SERPINE1 expression. Genes within these modules were then subjected to a GO enrichment analysis.

Statistical analysis. Statistical analyses were conducted using GraphPad Prism 10 (Dotmatics). The data are presented as the means ± SDs. Comparisons between groups were analyzed using a two-tailed Student's t test. For multiple comparisons, two-way ANOVA followed by Šídák's multiple comparisons test were performed. Significance levels were indicated as follows: $^{***}P<0.001$, $^{**}P<0.01$, $^{*}P<0.05$, and 'ns' indicated not significant. All experiments were performed in triplicate, unless noted otherwise. $P<0.05$ was considered to indicate a statistically significant difference.

Results

Prognostic significance and cellular functional states associated with SERPINE1. The present study explored the prognostic value of SERPINE1 by correlating its expression with the overall survival of patients with various cancers using GEPIA2 and TCGA data. A map of the HR of survival (Fig. 1A) revealed the prognostic significance of SERPINE1 across type of cancers. Notably, BRCA, LGG and SKCM showed distinct associations (Fig. 1B): A significant negative association was observed in LGG (Logrank P=2.4e-9), a borderline association was observed in BRCA (Logrank P=0.051), and a significant positive correlation was observed in SKCM (Logrank P=0.0065). SERPINE1 expression was markedly higher in LGG tissues than in normal tissues (Fig. 1C). At the single-cell level, SERPINE1 was related to distinct functional states in various types of cancer cell (Fig. 1D). These findings highlighted the differential prognostic relevance of SERPINE1 across type of cancers, probably because differently involved signaling pathways affect cell survival, proliferation, and invasion.

Diverse effects of SERPINE1 on cell proliferation. Variable effects of SERPINE1 on cell proliferation have been reported.

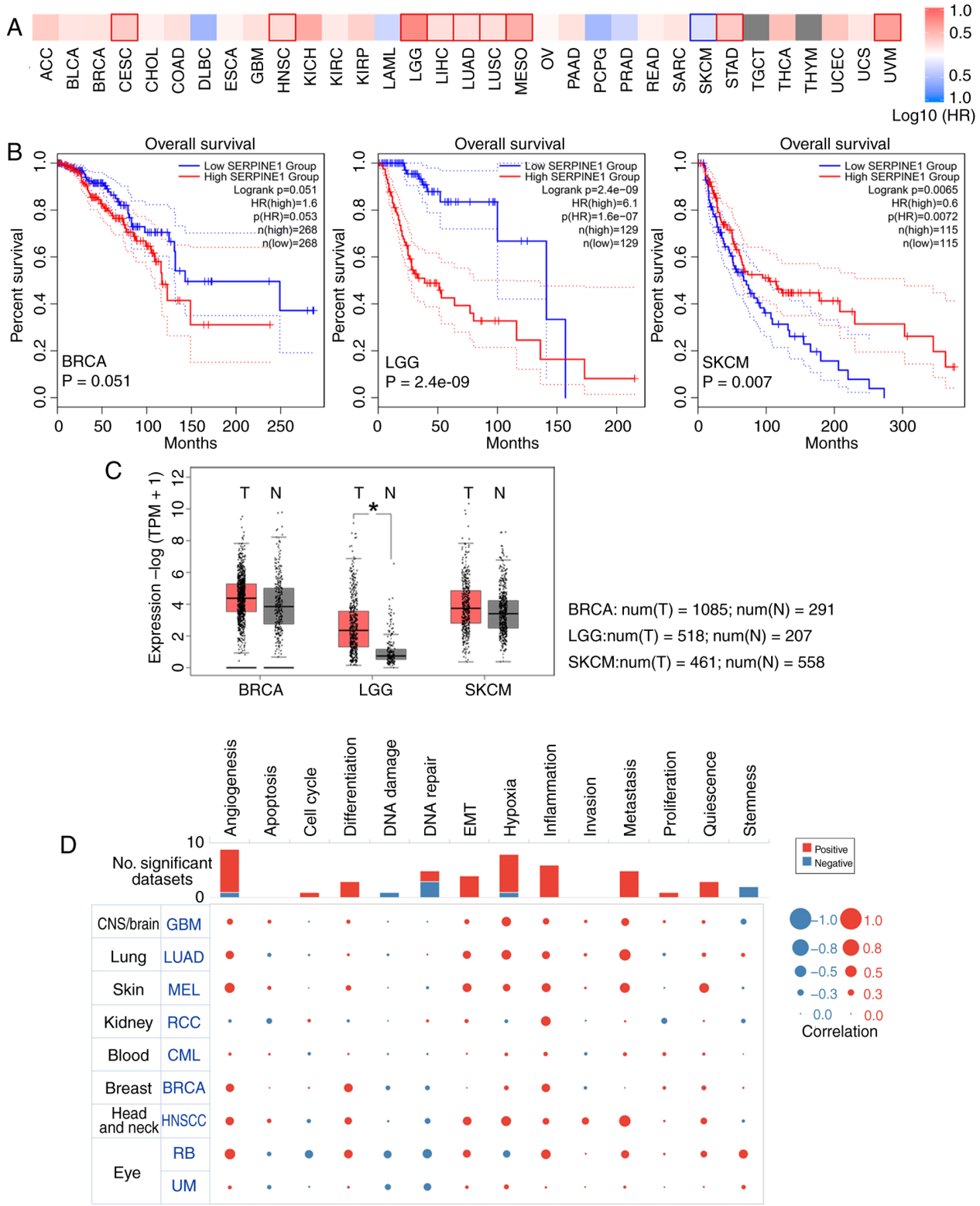

Figure 1. Prognostic significance and cellular functional states of SERPINE1. (A) Heatmap of survival (GEPIA2) showing the HRs for SERPINE1 expression across type of cancers (expression data and clinical survival data are sourced from The Cancer Genome Atlas projects. The cohort was split into two groups based on the expression level of SERPINE1. GEPIA2 employs a quartile-based cut-off: tumors with SERPINE1 expression levels at or above the 75th percentile are classified into the 'high expression' group, and those with SERPINE1 expression at or below the 25th percentile are classified into the 'low expression' group. This method minimizes the effects of outliers. Red and blue indicate higher and lower risks, respectively; highlighted boxes denote significant outcomes (P<0.05). (B) Kaplan-Meier curves for the significance of the effect of SERPINE1 on overall survival. The statistical significance of the difference between survival curves was computed using the log-rank (Mantel-Cox) test. The analysis outputs HR with its confidence interval and the log-rank P-value, all of which are annotated in the figure. (C) SERPINE1 expression in BRCA, LGG, and SKCM tumors compared with normal tissues (GEPIA2). For BRCA, there were 1,085 tumor samples and 291 normal samples; for LGG, 518 tumor samples and 207 normal samples; and for SKCM, 461 tumor samples and 558 normal samples. (D) Average correlation of SERPINE1 expression with functional states in cancers (CancerSEA database). Correlations with an absolute Spearman's ρ>0.3 and a Benjamini and Hochberg adjusted P-value (false discovery rate) <0.05 were considered significant. *P<0.05. SERPINE1, serine protease inhibitor clade e member 1; GEPIA2, gene expression profiling interactive analysis 2; HR, hazard ratio; BRCA, breast cancer; LGG, low-grade glioma; SKCM, skin cutaneous melanoma.

A total of three tumor cell lines (MDA-MB-231, H4 and C918) were selected for *in vivo* and *in vitro* studies. MDA-MB-231 (abbreviated as 231) cells, a widely established model, was chosen because of its aggressive triple-negative breast cancer phenotype and metastatic potential (33); the H4 glioma cell line, a commonly used model for brain tumor biology, has gene expression profiles similar to those of low-grade glioma, especially in terms of cell proliferation and invasion-related genes (34,35); and the cutaneous melanoma cell line C918 has notably high SERPINE1 expression levels (detected across melanoma cell lines in our laboratory; data not shown) and a high capacity for invasion and metastasis. Additionally, Yu *et al* (36) reported that this cell line harbors a BRAF (G464E) mutation and a KRAS (G12D) mutation. Western blotting showed that SERPINE1 expression was detected in all three cell lines. Knockdown was achieved using two distinct shRNA-expressing lentiviruses alongside a control lentivirus. Efficient knockdown was confirmed at the protein, mRNA and secretory protein levels (Figs. 2A and S1A-B). Compared with those in the controls (shc), the colony-forming efficiency and proliferation in the 231-shSE1 and H4-shSE1 cells decreased but that in the C918-shSE1 cells increased (Fig. 2B and S1C). A rescue experiment was conducted to further validate these findings. In SERPINE1-knockdown cells, the re-expression of an shRNA-resistant SERPINE1 construct rescued the levels of both the intracellular protein and secreted SERPINE1 (Fig. S1D). Consequently, the impaired clonogenic and proliferation abilities caused by SERPINE1 knockdown were reversed (Fig. S1E-F).

A subcutaneous xenograft mouse model was established. Compared with control mice (231-shc), reduced tumor volumes were observed in 231-shSE1 tumor-bearing mice. In contrast, increased tumor volumes were detected in C918-shSE1 tumor-bearing mice compared with their controls (C918-shc; Fig. 2C and D). The metastatic potential was further evaluated using a lung metastasis mouse model, which involved a tail vein injection of GFP-expressing cells. GFP expression was consistently maintained in all the cells (Fig. S1G). Notably, fewer lung metastatic nodules produced by 231-shSE1 and C918-shSE1 cells were detected than those produced by control cells. Lung nodule formation rate (defined as the number of mice with lung metastases per total number of injected mice) was: 4 of 6 for 231-shSE1 versus 5 of 6 for 231-shc; and 6 of 6 for both C918-shSE1 and C918-shc (Fig. 2E and F). H4 cells, which lack tumorigenic capacity, were excluded from the *in vivo* experiments. These results suggested that SERPINE1 can either promote or inhibit tumor cell proliferation *in vivo* and *in vitro*. Tumor metastasis is a complex, multistep process influenced by various factors and is not solely contingent on cell proliferation.

SERPINE1-mediated cell cycle regulation. The present study explored the mechanisms underlying the differences in cell proliferation by conducting an RNA-seq analysis to compare gene expression between the SERPINE1 knockdown and control groups of 231, H4 and C918 cells. DEGs were visualized in volcano plots (Fig. S2A). The GO enrichment analysis revealed key biochemical functions of these DEGs (Fig. 3A). Notably, in the comparison between C918-shSE1 and C918-shc cells, DEGs were markedly enriched for terms related to cell cycle regulation. These included 'Regulation of transcription involved in the G_1/S transition of the mitotic cell cycle', 'DNA strand elongation involved in DNA replication', 'Double-strand break repair via break-induced replication', 'DNA replication initiation' and 'DNA replication'. A heatmap displays the expression levels of the DEGs belonging to these enriched biological processes (Fig. 3B). Among these genes, minichromosome maintenance complex component 3 (MCM3), a key component of the DNA replication machinery, unwinds DNA at replication origins and is involved in the synthesis of new DNA strands during S phase. After replication, MCM3 is phosphorylated (p-MCM3) and dissociates from the nuclear structure (37,38). As detected by RNA-seq, MCM3 mRNA expression was 2.35-fold higher in C918-shSE1 cells than in control C918-shc cells (Fig. 3B). Western blotting analysis showed an increased ratio of p-MCM3 to total MCM3 protein in C918-shSE1 compared with C918-shc (Fig. 3C). In addition, the proportion of p-MCM3-positive cells was also higher in C918-shSE1-derived xenografts. However, SERPINE1 knockdown did not markedly affect MCM3 or p-MCM3 levels in 231 and H4 cells (Figs. 3C and S2B).

The effect of SERPINE1 knockdown on the cell cycle was then assessed. In C918-shSE1 cells, the proportion of cells in G_0/G_1 phase decreased markedly compared with the C918-shc control (P=0.02), while the proportion in G_2/M phase showed an increasing trend (P=0.1). No significant changes in cell cycle distribution were observed in either 231-shSE1 or H4-shSE1 cells compared with their respective shc controls (Fig. 3D). Furthermore, the present study profiled 89 cell cycle-related regulatory proteins using a protein array to elucidate the underlying molecular mechanisms in C918 cells. SERPINE1 knockdown in C918 cells decreased the levels of key regulatory proteins, including p53 and SMAD3 (Figs. 3E and S3A). RNA-seq analysis showed decreased mRNA levels of TGFB1, SMAD3, and CDKN1A/B/C and increased mRNA levels of CCND1 and CCNE1 in C918-shSE1 cells compared with those in control cells (Fig. 3F). Western blotting revealed reduced p53 and SMAD3 phosphorylation, increased Rb phosphorylation, increased cyclin D1 and cyclin E1 levels, and decreased p21 levels in C918-shSE1 cells (Fig. 3G). Given these findings, the present study sought to confirm that the observed cell cycle alterations were specifically due to SERPINE1 loss. In C918 cells with SERPINE1 knockdown, re-expression of an shRNA-resistant SERPINE1 construct reversed the alterations in the cell cycle distribution and the expression of associated regulatory proteins caused by SERPINE1 downregulation (Fig. S3B-D).

TGF-β acts as an upstream regulator of both SERPINE1 and the p53/SMAD3 pathway. Following SERPINE1 knockdown in C918 cells, TGF-β levels were reduced compared with those in control cells. Based on this finding, the present study treated SERPINE1-knockdown C918 cells with exogenous TGF-β1. The results showed that exogenous TGF-β1 supplementation reversed cell cycle progression and the corresponding changes in protein expression caused by SERPINE1 knockdown (Fig. S3E-F).

These results indicated that SERPINE1 plays a crucial role in C918 cell cycle progression by modulating p53 and SMAD3, which function downstream of the TGF-β pathway. Mechanistically, SERPINE1 may enhance upstream signaling

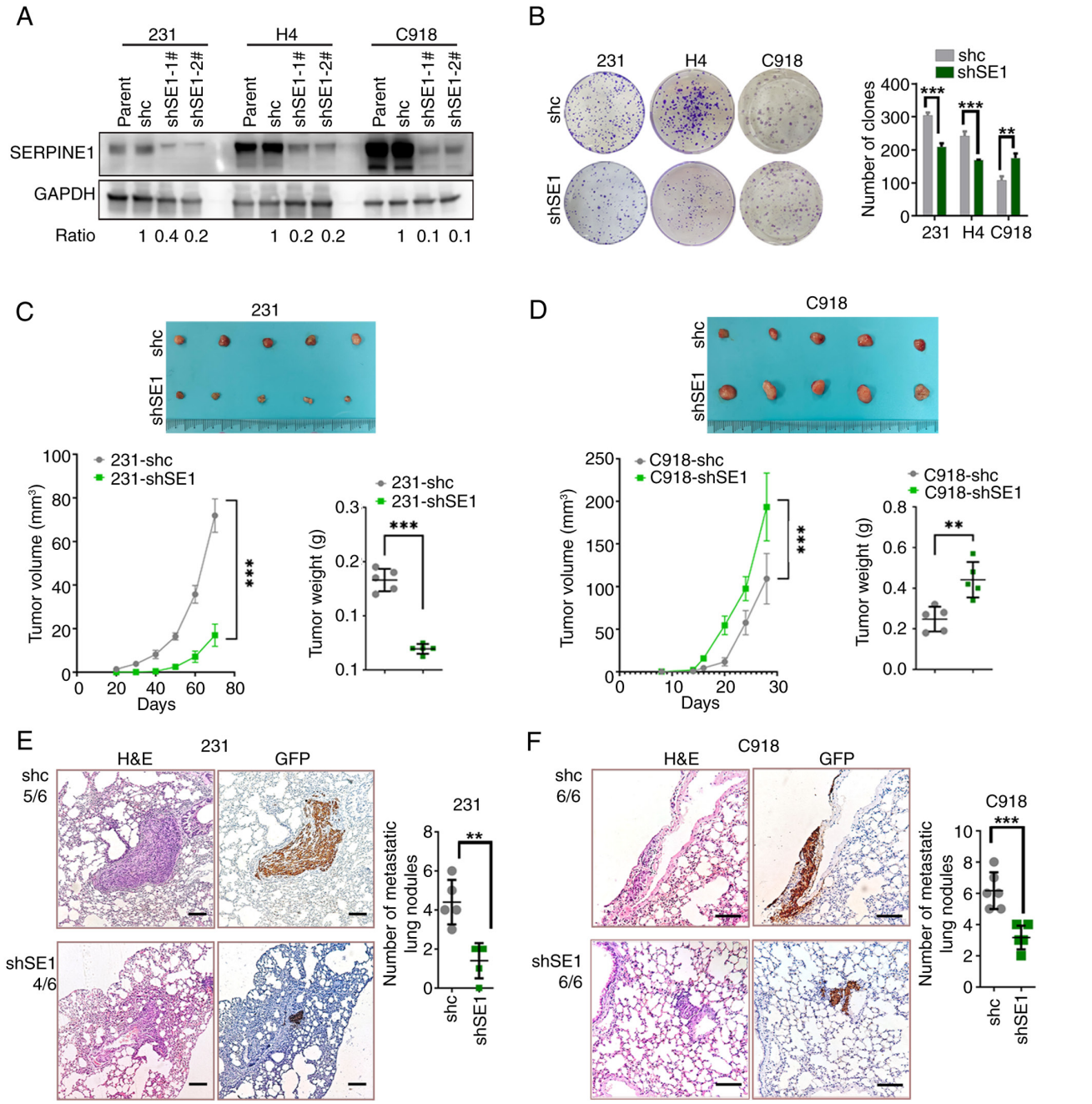

Figure 2. Diverse effects of SERPINE1 knockdown on cell proliferation. (A) Western blotting showing SERPINE1 protein levels in 231, H4, and C918 cells following transfection with the shSE1 and shc with GAPDH serving as the loading control. Band intensities were measured using ImageJ software and are presented as ratios. These ratios were calculated as (target protein/GAPDH levels) in the experimental group divided by those in the control group. Data represent mean ± SDs of three independent experiments. (B) Colony formation ability of shSE1 and control (shc) cells. Statistical significance was determined using a two-sided Student's t test. The data are presented as the means ± SDs of three independent experiments. (C-D) Xenograft tumors derived from (C) 231 and (D) C918 cells with shSE1 and shc cells; the tumor growth and weight were compared between shSE1 and shc groups. Statistical significance was determined using two-way ANOVA followed by Šídák's multiple comparisons test (tumor growth) and a two-sided Student's t test (tumor weight). The data are presented as the means ± SDs. n=5. (E-F) Lung metastatic foci in nude mice were stained with H&E and GFP (scale bar, 100 μm). The fractions (numerator/denominator) adjacent to the images represent the lung metastatic focus rate (defined as the number of mice with lung metastases per total number of injected mice). The lung metastatic focus rate was: 4 of 6 for 231-shSE1 versus 5 of 6 for 231-shc; and 6 of 6 for both C918-shSE1 and C918-shc. Statistical significance was determined using a two-sided Student's t test. The data are presented as the means ± SDs. n=6. ***P<0.001, **P<0.01. SERPINE1, serine protease inhibitor clade e member 1; shRNA, short hairpin RNA; shSE1, shRNA targeting SERPINE1; shc, shRNA scrambled control; H&E, hematoxylin and eosin staining; GFP, green fluorescent protein.

by promoting TGF-β1 generation, thereby resulting in a self-amplifying cascade effect.

SERPINE1-mediated modulation of the ERK/p38 ratio and anoikis. The mechanisms underlying the effects of SERPINE1 knockdown on the proliferation of 231 cells and H4 cells have not yet been elucidated. Given the influence of SERPINE1 on the uPA/uPAR axis, it may indirectly modulate cancer cell proliferation by affecting the balance between ERK activity and p38 activity (39-41). The present study aimed to evaluate

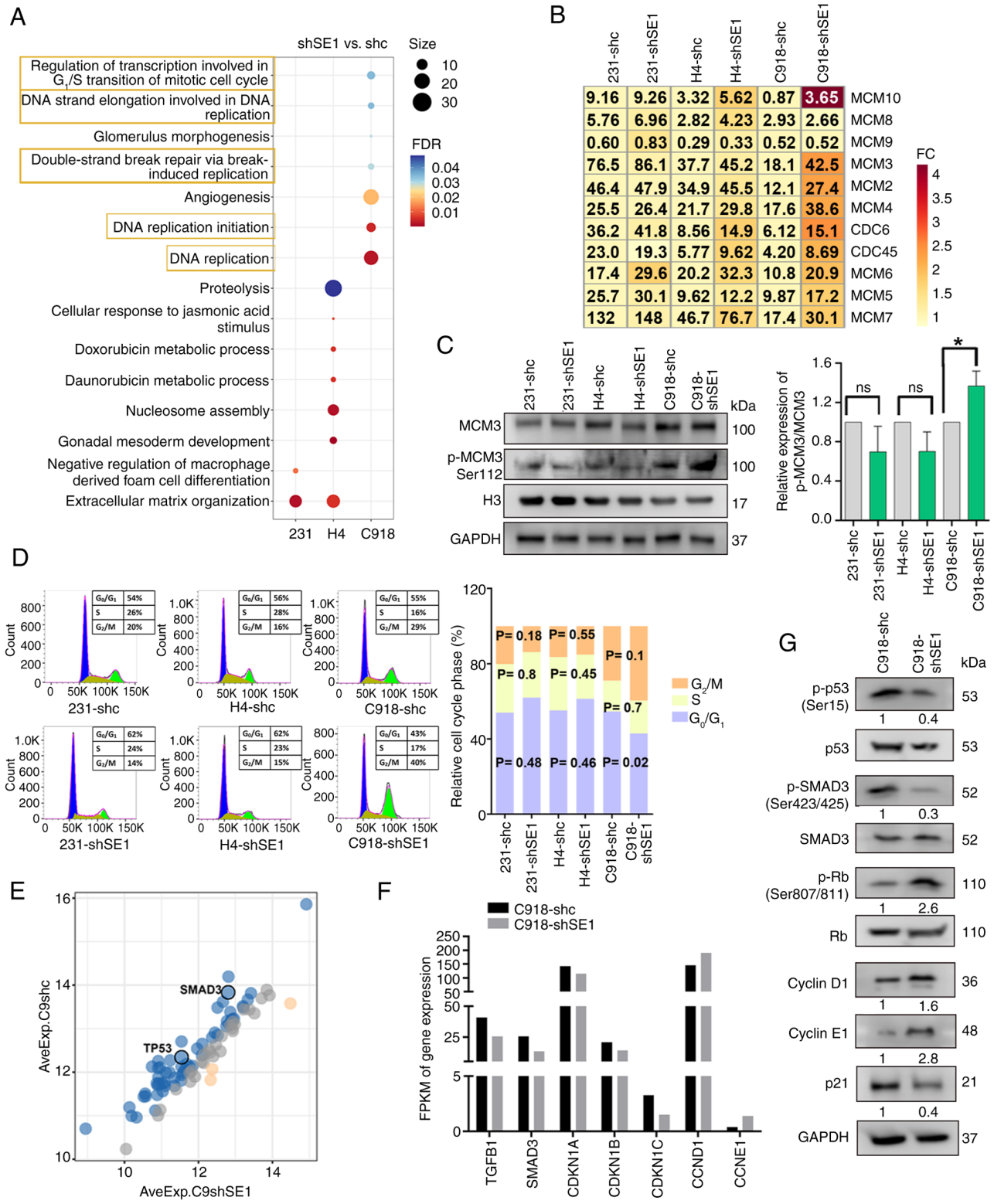

Figure 3. SERPINE1-mediated cell cycle regulation. (A) The GO enrichment analysis of DEGs obtained from RNA-seq revealed significant changes in biological processes after SERPINE1 knockdown between shSE1 and shc groups across three cell lines. RNA-seq was performed using one biological replicate per group. (B) Heatmap of DEGs associated with the highlighted processes in (A). (C) Western blotting was performed on nuclear and cytoplasmic extracts to detect MCM3 and p-MCM3 levels (histone H3 and GAPDH were used as controls). The relative levels of p-MCM3 and MCM3 were normalized to the expression of histone H3 and GAPDH, respectively. The relative p-MCM3/MCM3 ratio was subsequently calculated. Data represent mean ± SDs of three independent experiments. (D) Flow cytometry of the cell cycle phase distribution (G_0/G_1, S, and G_2/M phases). Statistical significance was determined using a two-sided Student's t test. The data are presented as the means ± SDs of three independent experiments. (E) Scatter plot of 89 cycle regulators from the protein array, highlighting SMAD3 and TP53. Blue indicates downregulated proteins (fold change ≥1.2); red indicates upregulated proteins (fold change ≤0.83); and grey indicates no change in the protein level. n=4 (F) RNA-seq data showing changes in the indicated gene expression between shSE1 and shc groups across three cell lines. RNA-seq was performed using one biological replicate per group. (G) Western blotting of the indicated proteins in C918 cells (shSE1 vs. shc). The ratios indicate the relative changes in the expression levels of the indicated proteins. Data represent mean ± SDs of three independent experiments. *P<0.05; ns, not significant. SERPINE1, serine protease inhibitor clade e member 1; GO, Gene Ontology; DEGs, differentially expressed genes; RNA-seq, RNA sequencing; shRNA, short hairpin RNA; shSE1, shRNA targeting SERPINE1; shc, shRNA scrambled control; FDR, false discovery rate; p-, phosphorylated.

the ratio of ERK/p38 activities, a known determinant of cancer cell proliferation or dormancy. SERPINE1 knockdown increased p-p38 levels in both 231 and H4 cells. In 231-shSE1 cells, p-ERK levels were markedly decreased, while no significant change was observed in H4-shSE1 cells. This decrease in the phosphorylation of these proteins reduced the ERK/p38 activity ratio in both 231-shSE1 and H4-shSE1 cells compared with their respective shc controls. No significant changes in p-ERK or p-p38 levels were detected in C918-shSE1 cells compared with the C918-shc control. Additionally, the levels of phosphorylated JNK and AKT, which markedly and variably affect cancer cell proliferation (42,43), remained unchanged following SERPINE1 downregulation (Fig. 4A).

Given that uPAR regulates the ERK/p38 pathway (40,44), the present study measured the protein and mRNA levels of uPAR. SERPINE1 downregulation reduced uPAR expression in 231 cells but not in H4 cells (Fig. 4B). Therefore, the present study further analyzed gene sets associated with SERPINE1 expression in BRCA, LGG and SKCM tumors using the GEPIA2 platform. The KEGG pathway enrichment analysis of the three gene sets revealed that the IL-17 signaling pathway was quite noticeably enriched in LGG (FDR=0.05), while it was not markedly enriched in BRCA (FDR=0.30) or SKCM (FDR=0.27; Fig. S4). Similarly, the KEGG pathway enrichment analysis of genes that were differentially expressed after SERPINE1 knockdown in the three cell lines revealed the unique enrichment of the IL-17 signaling pathway in H4 cells (Fig. S5). IL-17 signaling promotes p38 phosphorylation through the Act1-TRAF6 axis. HSP90α enhances this process by stabilizing Act1, thereby facilitating IL-17-mediated p38 activation (45,46). As predicted, the present study found that HSP90α protein and mRNA expression increased in H4-shSE1 cells but not in 231-shSE1 cells (Fig. 4B). Then, the present study tested the effects of uPAR and HSP90α on ERK/p38 activity and cell growth by overexpressing uPAR in 231-shSE1 cells and knocking down HSP90α in H4-shSE1 cells. The overexpression of uPAR in 231-shSE1 cells reversed the changes in the ERK/p38 activity ratio and cell growth, increasing p-ERK levels and decreasing p-p38 levels (Fig. 4C). HSP90α knockdown in H4-shSE1 cells modulated ERK/p38 signaling and cell proliferation by reducing p-p38 levels and increasing p-ERK levels (Fig. 4D).

To explore additional mechanisms, the present study used WGCNA to focus on SERPINE1-associated modules in TCGA datasets for BRCA, LGG and SKCM (Fig. S6A-E). Considering the role of the Wnt pathway in tumor stemness in BRCA and SKCM and the prominence of cellular differentiation pathways in LGG, the present study proceeded to examine changes in stemness *in vitro*. Cancer stem cells (CSCs), which are characterized by self-renewal and stem-like properties, can be modulated by SERPINE1 (47). Using a suspension culture of CSCs, the present study investigated the expression of the stemness marker CD133, a key CSC marker, across different tumor types. The percentage of CD133-positive cells was slightly increased in 231-shSE1 (mean 0.35 vs. 0.23%; P=0.001) and H4-shSE1 (mean 0.39 vs. 0.26%; P=0.014) cells and slightly decreased in C918-shSE1 cells (mean 0.94 vs. 1.65%; P=0.0003) compared with that in control cells (Fig. S7A). Given the low proportion of CD133-positive cells, further research is needed to determine whether these minor changes can affect the overall cell proliferation phenotype.

Considering that SERPINE1 is involved in cellular senescence and apoptosis, which also impact proliferation, the present study performed SA-β-galactosidase (SA-β-gal) staining and apoptosis assays on adherent cells. No significant differences in SA-β-gal positivity or apoptosis were detected between the SERPINE1 knockdown and control groups (Fig. S7B and C). These findings indicated that reducing SERPINE1 expression alone may not be adequate to induce cellular senescence and apoptosis in adherent cells.

Consequently, the present study explored anoikis in nonadherent suspension cultures and found that SERPINE1 downregulation markedly induced anoikis in 231 and H4 cells but not in C918 cells (Fig. 4E and F). Similarly, following the restoration of SERPINE1 expression, the alterations caused by SERPINE1 knockdown, including changes in the ERK/p38 ratio, the expression of uPAR and HSP90α, and anoikis were reversed (Fig. S8A-C). Overall, SERPINE1 downregulation promotes the proliferation of C918 cells by inducing cell cycle progression but inhibits the proliferation of 231 and H4 cells by altering the ERK/p38 balance and inducing anoikis.

Variable effects of SERPINE1 on cell migration and invasion. Multiple studies have established a role for SERPINE1 in promoting tumor migration and invasion (19-24). Corroborating this role, key motility-related KEGG pathways ('Regulation of actin cytoskeleton', 'Leukocyte transendothelial migration', and 'Focal adhesion') were enriched in high-SERPINE1 groups of BRCA, LGG, and SKCM (Fig. 5A). Then, the present study explored cell migration and invasion using the conventional Transwell method under *in vitro* conditions. In the Transwell migration assay, SERPINE1 knockdown inhibited the migration of 231, H4 and C918 cells in all the shSE1 groups compared with their respective shc controls (Fig. 5B). Furthermore, the present study assessed the capacity of cells to invade the extracellular matrix by performing a Transwell invasion assay in which the porous membrane was coated with Matrigel (a commonly used extracellular matrix comprising ~60% laminin, 30% type IV collagen, 8% entactin and some growth factors) and collagen I to allow invasive cells to migrate chemotactically. In chambers coated with Matrigel and collagen I, the number of cells that migrated through the Transwell membrane was decreased in 231-shSE1 and C918-shSE1 cells compared with the control group, whereas it was increased in H4-shSE1 cells, suggesting that downregulation of SERPINE1 enhances the invasive ability of H4 cells (Fig. 5C and D). In addition, after SERPINE1 expression was restored, the impairments in cell migration and invasion caused by SERPINE1 knockdown were reversed (Fig. S9A-C). These data suggested that the effects of SERPINE1 on cell migration and invasion are also controversial.

SERPINE1 regulates MMP and TIMP activities. The results of the invasion assay prompted a further investigation into the underlying mechanisms involved. MMPs, a family of enzymes, facilitate the degradation of extracellular matrix components, including collagen, elastin, fibronectin, laminin and proteoglycans (48). Due to their crucial roles in ECM proteolysis and cell motility, semiquantitative antibody arrays

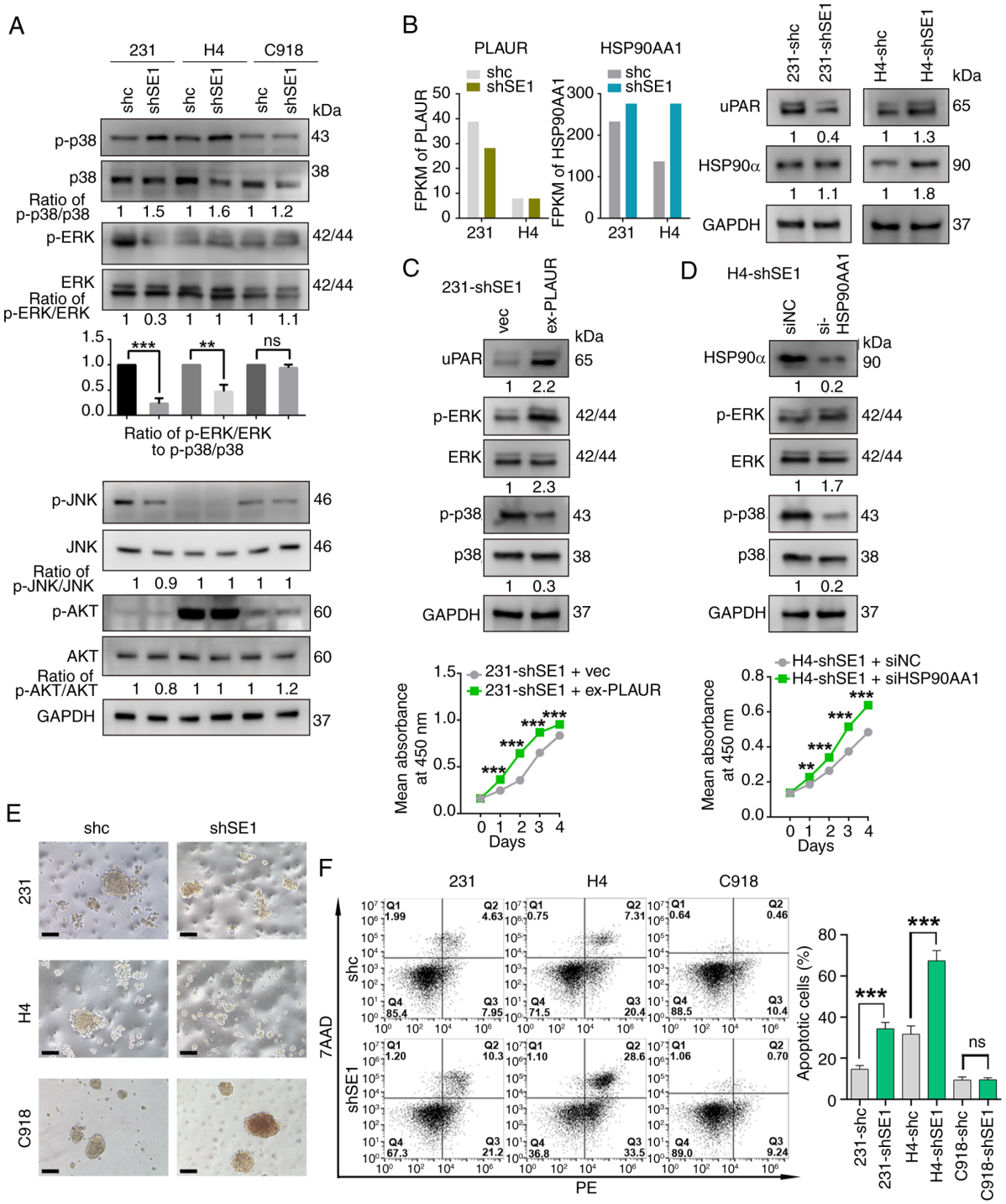

Figure 4. SERPINE1-mediated modulation of the ERK/p38 ratio and anoikis. (A) Upper panel: western blotting showing ERK, p-ERK, p38, and p-p38 levels. Quantitative data showed the p-ERK/ERK and p-p38/p38 ratios in SERPINE1 knockdown cells compared with control cells. Lower panel: western blotting analysis of p-AKT, AKT, p-JNK and JNK (normalized to total protein) levels in the shSE1 and shc groups. The numbers beneath the bands represent the ratios of the expression levels of the indicated proteins. Data represent mean ± SDs of three independent experiments. (B) PLAUR and HSP90AA1 mRNA and protein levels in shSE1 and shc cells analyzed using RNA-seq (left panel) and western blotting (right panel). The numbers beneath the bands represent the ratios of the expression levels of the indicated proteins and represent mean ± SDs of three independent experiments. RNA-seq was performed using one biological replicate per group. (C-D) Upper panel: (C) 231-shSE1 cells were infected with lentivirus containing PLAUR cDNA (ex-PLAUR) or the corresponding empty vector control (vec). (D) H4-shSE1 cells were transfected with siRNA targeting HSP90AA1 (si-HSP90AA1) or siNC. The expression levels of uPAR and HSP90α, as well as the activity of ERK and p38, were detected by western blotting, with GAPDH serving as the loading control. Data represent mean ± SDs of three independent experiments. Lower panel: Cell proliferation was assessed by CCK-8 assay in 231-shSE1 cells infected with ex-PLAUR or vec, and in H4-shSE1 cells transfected with si-HSP90AA1 or siNC. Statistical significance was determined using two-way ANOVA followed by Šídák's multiple comparisons test. The data are presented as the means ± SDs. n=6. (E) Morphology of shSE1 and shc cells cultured under suspension condition. (scale bar, 100 μm). (F) Apoptotic cells cultured under suspension condition were analyzed by flow cytometry following Annexin V-PE/7AAD staining (72 h of suspension culture). Statistical significance was determined using a two-sided Student's t test. The data are presented as the means ± SDs of three independent experiments. **P<0.01 ***P<0.001, ns, not significant. SERPINE1, serine protease inhibitor clade e member 1; p-, phosphorylated; shRNA, short hairpin RNA; shSE1, shRNA targeting SERPINE1; shc, shRNA scrambled control; PLAUR, plasminogen activator, urokinase receptor; HSP90AA1, heat shock protein 90 alpha family class a member 1; RNA-seq, RNA sequencing; vec, empty vector control; siRNA, short interfering RNA; siNC, negative control siRNA; uPAR, urokinase-type plasminogen activator receptor; HSP90α, heat shock protein 90-alpha.

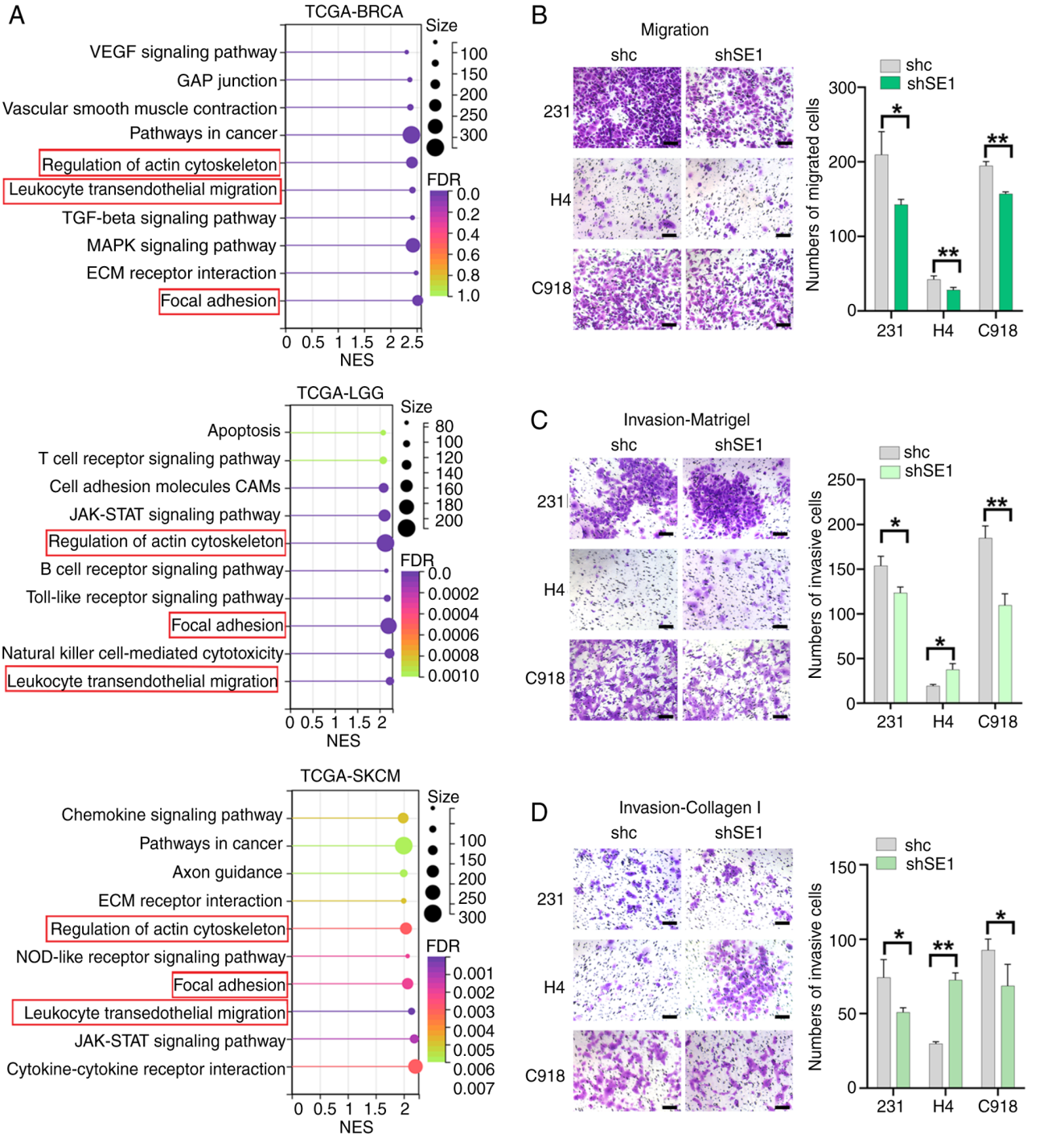

Figure 5. Variable effects of SERPINE1 on cell migration and invasion. (A) KEGG enrichment analysis via GSEA comparing high and low SERPINE1 expression in BRCA, LGG, and SKCM (TCGA dataset). Representative images and quantification of Transwell assays of the migration (B) of shSE1 and shc cells. Representative images and quantification of Transwell invasion assays through (C) Matrigel and (D) collagen type I. Cells from three random fields in triplicate wells were counted. Scale bar, 100 μm. Statistical significance was determined using a two-sided Student's t test. The data are presented as the means ± SDs of three independent experiments. **P<0.01, *P<0.05. SERPINE1, serine protease inhibitor clade e member 1; KEGG, Kyoto Encyclopedia of Genes and Genomes; GSEA, gene set enrichment analysis; BRCA, breast cancer; LGG, low-grade glioma; SKCM, skin cutaneous melanoma; TCGA, The Cancer Genome Atlas; NES, normalized enrichment score; FDR, false discovery rate.

were used to analyze the expression profiles of seven MMPs and three TIMPs in cell supernatants. To this end, the present study found that SERPINE1 knockdown differentially altered MMP/TIMP levels across cell lines: in the 231-shSE1 group, levels of MMP-1, -9, -10, and -13 decreased relative to the 231-shc control; in the H4-shSE1 group, levels of MMP-1 and TIMP-2 increased, while those of MMP-2, -8, -13, and TIMP-4 decreased compared with the H4-shc control; in the C918-shSE1 group, levels of MMP-1, -3, -10, and -13 decreased relative to the C918-shc control (Fig. 6A). Notably, MMP-1 expression was reduced in 231-shSE1 and C918-shSE1 cells but increased in H4-shSE1 cells and MMP-13 expression was consistently reduced in all the SERPINE1 knockdown groups. To confirm the activity results of these two MMPs, the

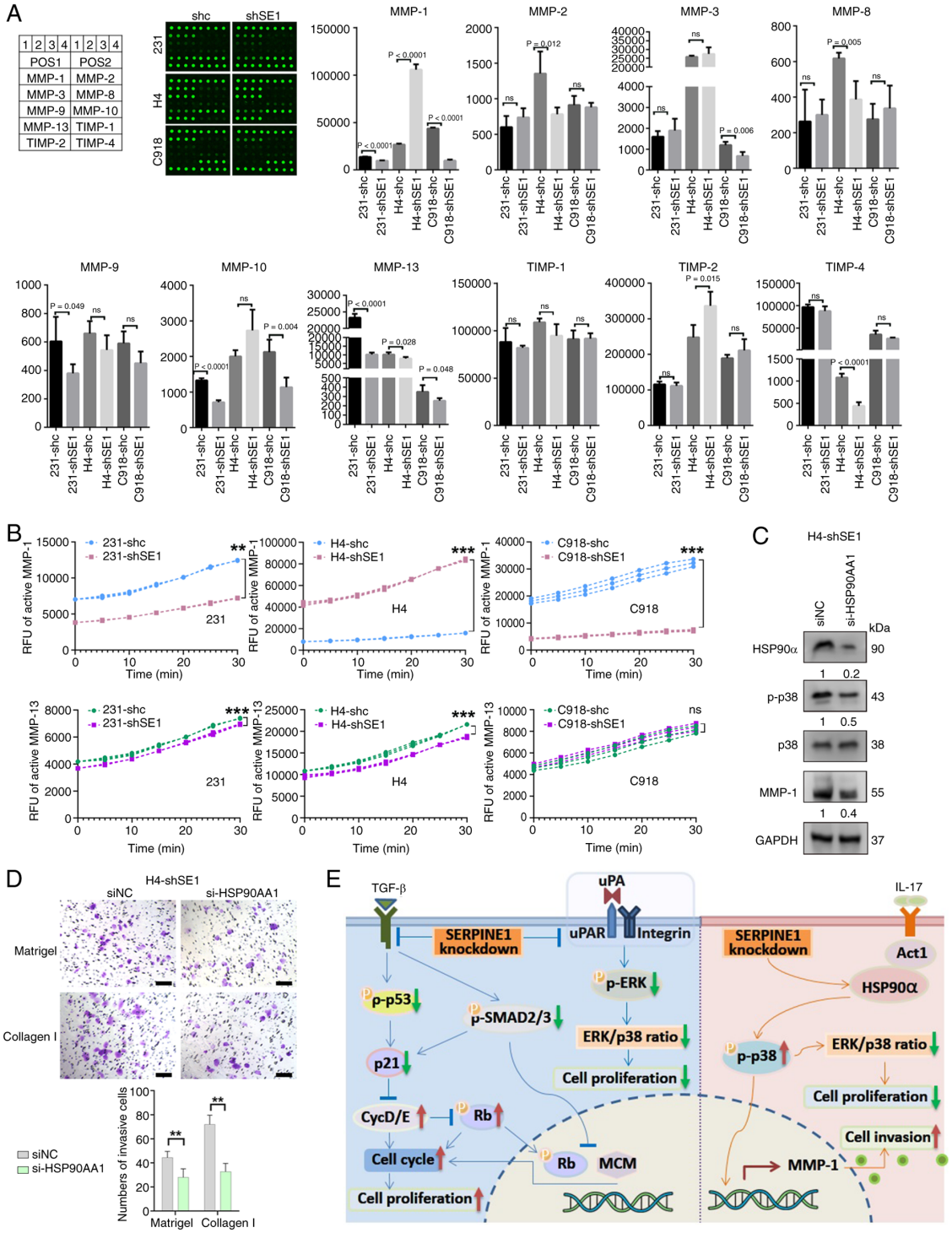

Figure 6. SERPINE1 regulates MMP activity. (A) MMP and TIMP levels in the supernatants of shSE1 and shc cells after 24 h of incubation and 10-fold concentration. Statistical significance was determined using a two-sided Student's t test. The data are presented as the means ± SDs. n=4. (B) Quantification of active MMP-1 and MMP-13 levels in cell lysates using fluorescence ELISA. Statistical significance was determined using two-way ANOVA followed by Šídák's multiple comparisons test. The data are presented as the means ± SDs of three independent experiments. (C) Western blotting showing the levels of the indicated proteins in H4-shSE1 cells at 72 h after transfection with the si-HSP90AA1 or siNC. The numbers beneath the bands represent the ratios of the expression levels of the indicated proteins and represent mean ± SDs of three independent experiments. (D) Representative images and quantification of Transwell invasion assays through Matrigel and collagen type I in H4-shSE1 cells transfected with the si-HSP90AA1 or siNC (scale bar, 100 μm). Statistical significance was determined using a two-sided Student's t-test. The data are presented as the means ± SDs of three independent experiments. (E) Diagram showing the mechanisms underlying the effects of SERPINE1 on cancer proliferation and invasion. SERPINE1 knockdown influences cell proliferation and invasion through distinct signaling pathways. With respect to proliferation, SERPINE1 knockdown reduces TGF-β levels, and this reduction alters the activity of SMAD3, p53, and MCM3 to promote cell cycle progression. SERPINE1 knockdown interferes with the uPAR-mediated balance of the ERK/p38 ratio; it may also affect this ratio by modulating HSP90α expression and p38 activity, which suppress cell proliferation. In terms of invasion, SERPINE1 downregulation increases MMP-1 levels via the HSP90α-p38 pathway, thereby promoting cellular invasion. ***P<0.001, **P<0.01, ns, not significant. SERPINE1, serine protease inhibitor clade e member 1; MMP, matrix metalloproteinases; TIMP, tissue inhibitors of metal proteases; shRNA, short hairpin RNA; shSE1, shRNA targeting SERPINE1; si, short interfering RNA; siHSP90AA1, short interfering heat shock protein 90 alpha family class a member 1; NC, negative control; uPAR, urokinase-type plasminogen activator receptor; p-, phosphorylated; MCM3, minichromosome maintenance complex component 3; HSP90α, heat shock protein 90-alpha.

present study subsequently quantified the levels of MMP-1 and MMP-13 activity using a fluorescent ELISA. Results showed that MMP-1 activity was markedly decreased in 231-shSE1 and C918-shSE1 cells compared with the control group, whereas it was increased in H4-shSE1 cells. For MMP-13 activity, a decrease was observed in 231-shSE1 and H4-shSE1 cells relative to controls; however, no significant difference was found between the knockdown group and the control group in C918 cells (Fig. 6B). Following the restoration of SERPINE1 expression, the reduced activity of MMP-1 and MMP-13 caused by SERPINE1 knockdown was reversed (Fig. S10). Although SERPINE1 downregulation in H4 cells induced complex alterations in the levels of MMPs and TIMPs, the net effect was an increase in cellular invasiveness. This outcome might be predominantly attributed to the increased levels of MMP-1, which could override the combined effects of other altered MMPs and TIMPs on governing cell invasion.

The activity of MMP-1, a key collagenase, is critical for collagen degradation and tumor progression. Its expression is regulated by growth factors, hormones, and cytokines, including those in the IL-17 pathway. HSP90α modulates the IL-17 pathway and stimulates MMP-1 expression via p38-mediated transcription (49,50). This previously established regulatory axis may account for our observations. Indeed, RNA-seq revealed a twofold increase in HSP90AA1 mRNA expression in H4-shSE1 cells compared with controls (Fig. S11). Furthermore, western blotting analysis showed increased p-p38 levels. Together, these results suggested that the upregulation of MMP-1 expression in H4-shSE1 cells may be mediated by the HSP90α-p38 axis. Consistent with this interpretation, this finding was confirmed by siRNA-mediated knockdown of HSP90α, which reduced p-p38 and MMP-1 levels (Fig. 6C), supporting the role of the HSP90α-p38 axis in regulating MMP-1 expression. Additionally, HSP90α knockdown reversed the invasion-enhancing effect of SERPINE1 downregulation on H4 cells (Fig. 6D).

Discussion

The differential effect of a single gene on various types of tumor, which occasionally exerts opposing effects, poses a significant challenge in oncological research. The relatively poor correlation between gene expression levels and their associated biological effects raises the question of which factors dictate these divergent outcomes. The present study focused on the role of SERPINE1 in cell proliferation and invasion (Fig. 6E). It showed that SERPINE1 downregulation suppressed the proliferation of 231 and H4 cells via uPAR- and HSP90α-mediated pathways, respectively, which decreased the ERK/p38 activity ratio. Moreover, SERPINE1 downregulation increased proliferation and cell cycle progression in C918 cells by inhibiting p53 and SMAD3 activities and partially disrupting MCM3 function. SERPINE1 downregulation decreased the invasiveness of 231 and C918 cells, increased the invasiveness of H4 cells and altered the expression and activity of certain MMPs and TIMPs. Specifically, MMP-1 levels were decreased in 231 and C918 cells but were increased in H4 cells. Notably, the HSP90α-p38 pathway mediated the upregulation of MMP-1 in H4 cells. Given the diverse roles of SERPINE1, the development of SERPINE1 inhibitors for various types of tumor requires careful consideration.

In the present study, SERPINE1 knockdown promoted growth and cell cycle progression of C918 cells by decreasing the phosphorylation of p53 and SMAD3 (crucial transcription factors in the TGF-β pathway) and subsequently upregulating the expression of cell cycle-related proteins. These findings contradict those of a previous study (14) indicating that SERPINE1 facilitates G_1 to S phase progression. Notably, SERPINE1 is a major target gene of TGF-β/p53. Moreover, the suppression of p53 resulted in the downregulation of SERPINE1 mRNA and protein levels. SERPINE1 also induced apoptosis in senescent type II pneumocytes by upregulating p53 expression, suggesting the formation of a reciprocal amplification loop between p53 and SERPINE1 (18,51). Additionally, exogenous SERPINE1 is sufficient to trigger TGF-β production, which in turn upregulates SERPINE1 expression, establishing a positive feed-forwards loop within the SERPINE1/TGF-β signaling pathway (16,52). Although the molecular mechanisms underlying the regulatory effects of SERPINE1 on TGF-β and p53 expression have not yet been fully elucidated, the present study provided novel insights, as it reveals that SERPINE1 knockdown can promote cell cycle progression via alternative pathways in a target gene-dependent manner.

Notably, SERPINE1 knockdown resulted in the upregulation of the expression of multiple MCM proteins at the transcript level. The MCM protein family, comprising six evolutionarily conserved subunits, is essential for initiating DNA replication and functions as a DNA helicase during the replication elongation phase. A study suggests that SERPINE1 overexpression inhibits hepatitis C virus replication, possibly mediated by the TGF-β signaling pathway (53). Specifically, TGF-β1 prevents S phase entry and induces cell cycle arrest by inhibiting the dissociation of the Rb-MCM complex (54). These studies corroborate the present findings that SERPINE1 downregulation is associated with reduced SMAD3 activity and cell cycle progression, indicating that SERPINE1 may modulate MCM activity via TGF-β, thereby exerting a multifaceted effect on the cell cycle.

The ERK/p38 signaling axis represents a crucial balanced mechanism that determines whether cells undergo proliferation or dormancy during cancer progression. This inverse relationship acts as a molecular switch controlling cancer cell fate: Dominant ERK signaling promotes proliferation and invasion, largely through sustained cyclin D1 expression, whereas predominant p38 activation induces cell cycle arrest and tumor dormancy (39). Consistent with this role, high uPAR expression has been shown to maintain an elevated ERK/p38 activity ratio, thereby generating strong mitogenic signals that drive cell cycle progression (40). In support of this mechanism, Xue *et al* (44) demonstrated that in pancreatic ductal adenocarcinoma cell lines, treatment with uPAR siRNA substantially reduced phosphorylated ERK levels but increased phosphorylated p38 levels. SERPINE1 knockdown decreased the ratio of active ERK to active p38 in 231-shSE1 cells, with p-ERK levels more markedly reduced than the levels of p38 phosphorylation. These observations may be attributed to the indirect effects of SERPINE1 on cancer cell proliferation through its interactions with uPA and uPAR, which incorporate β1 integrins, stimulate cancer cell growth

and promote the transition from dormancy by activating focal adhesion kinase and the ERK signaling pathway. Genes such as uPA, uPAR, SERPINE1 and MMPs are targets of TGF-β1 and exhibit positive feedback within the SERPINE1/TGF-β signaling pathway (16,52,55). Consistent with these findings, the present study showed that the overexpression of PLAUR restored the ERK/p38 ratio and cell growth.

In H4 cells, SERPINE1 knockdown markedly decreased p38 phosphorylation, whereas ERK phosphorylation remained largely unchanged. Unlike 231-shSE1 cells, in which reduced transcription levels of PLAU and PLAUR were detected, no significant alterations in PLAU and PLAUR mRNA levels were observed in H4-shSE1 cells. Therefore, the present study analyzed gene sets related to SERPINE1 expression in BRCA, LGG and SKCM tumors to identify enriched signaling pathways. Notably, the IL-17 signaling pathway was markedly enriched in LGG. Similarly, the KEGG pathway enrichment analysis of DEGs after SERPINE1 knockdown in the three cell lines revealed the unique enrichment of the IL-17 signaling pathway in H4 cells. Lin *et al* (56) reported that interleukin-17D drives lung cancer progression by engaging the p38 MAPK pathway to recruit tumor-associated macrophages. Xiang *et al* (57) reported that IL-17 enhances the self-renewal of ovarian CD133(+) CSLCs via the NF-κB and p38 MAPK pathways, as evidenced by the activation of both signaling molecules upon IL-17 stimulation. IL-17 has been shown to promote p38 phosphorylation via the Act1-TRAF6 axis (46,58,59). HSP90α stabilizes Act1, enhancing this process and facilitating IL-17-mediated p38 activation. Consistent with these findings, an analysis of the H4-shSE1 cell RNA-seq revealed that the upregulation of the expression of the HSP90α gene and downregulation of HSP90α expression in H4-shSE1 cells transfected with a small interfering RNA reversed the changes in the ERK/p38 ratio and cell growth. To date, no studies have reported direct or indirect interactions between SERPINE1 and HSP90α. Tomcik *et al* (60) showed that HSP90 expression was increased in a TGF-β-dependent manner, suggesting that SERPINE1 downregulation may lead to reduced TGF-β levels through a feedback mechanism, consequently decreasing HSP90α expression.

Additionally, in contrast to the 231 cells and H4 cells used in the present study, the C918 cells seem to be an exception to the regulation of cell proliferation and dormancy by ERK/p38 signaling. It may developed a resistance strategy to bypass the antiproliferative effects of increased p38 activity, despite having high levels of ERK and p38 (40,61). The role of SERPINE1 in regulating apoptosis has been explored in several previous studies. It stimulates anoikis by impairing cell adhesion to vitronectin and resistance to apoptosis when cells migrate to other extracellular matrix proteins by inhibiting intrinsic and extrinsic apoptotic pathways and promoting AKT- and ERK-mediated survival pathways (62-66). The present study confirmed this finding in the suspension cultures of 231 and H4 cells but not in C918 cells. Multiple factors influencing resistance to anoikis have been identified (67). Weems *et al* (68) recently showed that dynamic blebbing on the plasma membrane promotes melanoma cell resistance to anoikis by initiating the survival-promoting effects of NRAS signaling pathways. The present finding that C918 cells harboring the KRAS (G12D) oncogene remain resistant to SERPINE1 knockdown-induced anoikis in suspension culture may be due to dynamic blebbing, a common morphological response in aggressive melanoma.

Studies have shown that SERPINE1 promotes tumor cell migration and invasion. SERPINE1 knockdown restrained the migration of differentiated thyroid cancer cells (69). Induced secretion of SERPINE1 led to increased MMP-1 levels and cell motility in human colon and liver cancer cell lines (70). SERPINE1 inhibition reduced cell spreading by modulating cell-substrate attachment and migration in glioblastoma cells (21). However, some studies have reported divergent or even contradictory outcomes, such as the role of SERPINE1 in mediating the formation of fibrotic adhesions in injured flexor tendons by suppressing MMP activity (29). Additionally, treatment with a SERPINE1 inhibitor increases the membrane-type MMP-1-dependent motility of chronic myeloid leukemia stem cells (66). In the present study, SERPINE1 downregulation inhibited the migration of three cell lines. Interestingly, SERPINE1 downregulation reduced the invasion of 231 and C918 cells but increased H4 cell invasion by markedly upregulating MMP-1 expression and activity via the HSP90α-p38 axis. Although this mechanism has not been previously reported, some supportive hints and relevant associations can be identified in existing literature. Wu *et al* (71) indicated that p38 activity is crucial for the ability of IL-17A/IL-17RA to promote NSCLC metastasis. Wu *et al* (72) reported that IL-17A facilitates human periodontal ligament fibroblast migration by upregulating the expression of MMP-1, which is mediated by the IL-17 receptor, p38 MAPK, and NF-κB pathways. Shibabaw *et al* (73) identified that the IL-17A/NF-κB/MMP axis promotes bone-metastatic breast cancer. The mechanism by which SERPINE1 affects the IL-17 signaling pathway remains unclear; however, the unique effect of the IL-17 pathway on H4 cells may explain their distinct behavior compared with that of the other two cell lines. Additionally, although the expression of TIMP-2, an inhibitor of MMPs, increases alongside that of MMP-1, it did not counteract the net proinvasive effect of SERPINE1 downregulation in H4 cells.

Extensive evidence has established that SERPINE1 plays key roles in tumor invasion, metastasis and angiogenesis, indicating that SERPINE1 is a promising therapeutic target in specific types of cancers. The development of various targeting approaches, ranging from conventional small-molecule inhibitors to novel miRNA-mediated modulators, reflects the broad and versatile potential of SERPINE1-targeted therapy. However, the biological complexity of SERPINE1 presents significant challenges. It operates within intricate signaling networks, interacts with multiple binding partners and is influenced by feedback mechanisms that can produce opposing biological effects, complicating its direct targeting. Further considerations include its concentration-dependent biphasic activity, context-dependent functional switching and unpredictable outcomes arising from pathway pleiotropy (11,66,74). Therefore, integrating molecular profiling through precision oncology to inform the design of rational multitarget therapies may be essential. Shifting from a reactive to a predictive treatment paradigm in this way could increase antitumor efficacy while minimizing adverse effects.

The present study had several limitations. First, the conclusions are derived from analyses across three models. While these findings provide some evidence, incorporating a broader panel of cell lines in future work would further strengthen and generalize these findings. Second, the phenotypes observed in the present study reflect the net effect of SERPINE1 operating in both intracellular and extracellular compartments; accordingly, correlating extracellular SERPINE1 levels with functional outcomes would be valuable for distinguishing its compartment-specific contributions. Third, further studies are needed to elucidate how SERPINE1 affects the IL-17 signaling pathway and how MCM specifically regulates cell cycle progression.

In conclusion, the present study explored the diverse roles of SERPINE1 in cell proliferation and invasion via distinct mechanisms. This understanding of complex regulatory networks provides a more nuanced perspective on SERPINE1 function, moving beyond simplistic oncogene or tumor suppressor classifications. Thus, these insights remain valuable for developing precise therapeutic strategies and advancing personalized medicine, with broader validation representing a key future direction.

Acknowledgements

The authors thank RayBiotech Biotechnology Co., Ltd. (Guangzhou, China) for providing services and data analysis related to the detection of cell cycle-related proteins and MMP arrays.

Funding

The present study was supported by the National Natural Science Foundation of China (grant no. 82002901).

Availability of data and materials

The sequence data generated in the present study may be found in the Gene Expression Omnibus (GEO) with the primary accession code GSE300877 or at the following URL: https://www.ncbi.nlm.nih.gov/geo/query/acc.cgi?acc=GSE300877.

Authors' contributions

WW curated the data, conducted the investigation and validation, and wrote the original draft. PZ curated the data and conducted the investigation and validation. TW performed validation. WW conducted validation and formal analysis. JL performed validation. QH was responsible for conceptualization, supervision and project administration. JM contributed to conceptualization, funding acquisition, investigation, methodology, validation, and writing, review and editing. WW and JM confirm the authenticity of all the raw data. All authors read and approved the final manuscript.

Ethics approval and consent to participate

All animal experimental protocols were carried out in accordance with the guidelines and regulations of the Institutional Animal Care and Use Committee at Tianjin Medical University (approval no. TMUaMEC 2022045).

Patient consent for publication

Not applicable.

Competing interests

The authors declare that they have no competing interests.

References

1. Peters L, Venkatachalam A and Ben-Neriah Y: Tissue-predisposition to cancer driver mutations. Cells 13: 106, 2024.
2. Wu K, El Zowalaty AE, Sayin VI and Papagiannakopoulos T: The pleiotropic functions of reactive oxygen species in cancer. Nat Cancer 5: 384-399, 2024.
3. Colak S and Ten Dijke P: Targeting TGF-β signaling in cancer. Trends Cancer 3: 56-71, 2017.
4. Boutelle AM and Attardi LD: p53 and tumor suppression: It takes a network. Trends Cell Biol 31: 298-310, 2021.
5. Schneider G, Schmidt-Supprian M, Rad R and Saur D: Tissue-specific tumorigenesis: Context matters. Nat Rev Cancer 17: 239-253, 2017.
6. Hoadley KA, Yau C, Hinoue T, Wolf DM, Lazar AJ, Drill E, Shen R, Taylor AM, Cherniack AD, Thorsson V, *et al*: Cell-of-origin patterns dominate the molecular classification of 10,000 tumors from 33 types of cancer. Cell 173: 291-304 e296, 2018.
7. Poulin EJ, Bera AK, Lu J, Lin YJ, Strasser SD, Paulo JA, Huang TQ, Morales C, Yan W, Cook J, *et al*: Tissue-specific oncogenic activity of KRAS(A146T). Cancer Discov 9: 738-755, 2019.
8. Lijnen HR: Pleiotropic functions of plasminogen activator inhibitor-1. J Thromb Haemost 3: 35-45, 2005.
9. Li L, Li F, Xu Z, Li L, Hu H, Li Y, Yu S, Wang M and Gao L: Identification and validation of SERPINE1 as a prognostic and immunological biomarker in pan-cancer and in ccRCC. Front Pharmacol 14: 1213891, 2023.
10. Kubala MH and DeClerck YA: The plasminogen activator inhibitor-1 paradox in cancer: A mechanistic understanding. Cancer Metastasis Rev 38: 483-492, 2019.
11. Sillen M and Declerck PJ: A narrative review on plasminogen activator inhibitor-1 and its (Patho)physiological role: To target or not to target? Int J Mol Sci 22: 2721, 2021.
12. Kwaan HC, Wang J, Svoboda K and Declerck PJ: Plasminogen activator inhibitor 1 may promote tumour growth through inhibition of apoptosis. Br J Cancer 82: 1702-1708, 2000.
13. Che Y, Wang J, Li Y, Lu Z, Huang J, Sun S, Mao S, Lei Y, Zang R, Sun N and He J: Cisplatin-activated PAI-1 secretion in the cancer-associated fibroblasts with paracrine effects promoting esophageal squamous cell carcinoma progression and causing chemoresistance. Cell Death Dis 9: 759, 2018.
14. Giacoia EG, Miyake M, Lawton A, Goodison S and Rosser CJ: PAI-1 leads to G1-phase cell-cycle progression through cyclin D3/cdk4/6 upregulation. Mol Cancer Res 12: 322-334, 2014.
15. Soeda S, Koyanagi S, Kuramoto Y, Kimura M, Oda M, Kozako T, Hayashida S and Shimeno H: Anti-apoptotic roles of plasminogen activator inhibitor-1 as a neurotrophic factor in the central nervous system. Thromb Haemost 100: 1014-1020, 2008.
16. Gifford CC, Lian F, Tang J, Costello A, Goldschmeding R, Samarakoon R and Higgins PJ: PAI-1 induction during kidney injury promotes fibrotic epithelial dysfunction via deregulation of klotho, p53, and TGF-beta1-receptor signaling. FASEB J 35: e21725, 2021.
17. Kortlever RM and Bernards R: Senescence, wound healing and cancer: The PAI-1 connection. Cell Cycle 5: 2697-2703, 2006.
18. Jiang C, Liu G, Luckhardt T, Antony V, Zhou Y, Carter AB, Thannickal VJ and Liu RM: Serpine 1 induces alveolar type II cell senescence through activating p53-p21-Rb pathway in fibrotic lung disease. Aging Cell 16: 1114-1124, 2017.
19. Brooks TD, Slomp J, Quax PH, De Bart AC, Spencer MT, Verheijen JH and Charlton PA: Antibodies to PAI-1 alter the invasive and migratory properties of human tumour cells in vitro. Clin Exp Metastasis 18: 445-453, 2000.
20. Liu G, Shuman MA and Cohen RL: Co-expression of urokinase, urokinase receptor and PAI-1 is necessary for optimum invasiveness of cultured lung cancer cells. Int J Cancer 60: 501-506, 1995.

21. Seker F, Cingoz A, Sur-Erdem İ, Erguder N, Erkent A, Uyulur F, Selvan ME, Gümüş ZH, Gönen M, Bayraktar H, *et al*: Identification of SERPINE1 as a regulator of glioblastoma cell dispersal with transcriptome profiling. Cancers (Basel) 11: 1651, 2019.
22. Hirahata M, Osaki M, Kanda Y, Sugimoto Y, Yoshioka Y, Kosaka N, Takeshita F, Fujiwara T, Kawai A, Ito H, *et al*: PAI-1, a target gene of miR-143, regulates invasion and metastasis by upregulating MMP-13 expression of human osteosarcoma. Cancer Med 5: 892-902, 2016.
23. Zhang W, Xu J, Fang H, Tang L, Chen W, Sun Q, Zhang Q, Yang F, Sun Z, Cao L, *et al*: Endothelial cells promote triple-negative breast cancer cell metastasis via PAI-1 and CCL5 signaling. FASEB J 32: 276-288, 2018.
24. Lin X, Lin BW, Chen XL, Zhang BL, Xiao XJ, Shi JS, Lin JD and Chen X: PAI-1/PIAS3/Stat3/miR-34a forms a positive feedback loop to promote EMT-mediated metastasis through Stat3 signaling in non-small cell lung cancer. Biochem Biophys Res Commun 493: 1464-1470, 2017.
25. Inoue M, Sawada T, Uchima Y, Kimura K, Nishihara T, Tanaka H, Yashiro M, Yamada N, Ohira M and Hirakawa K: Plasminogen activator inhibitor-1 (PAI-1) gene transfection inhibits the liver metastasis of pancreatic cancer by preventing angiogenesis. Oncol Rep 14: 1445-1451, 2005.
26. Hjortland GO, Bjørnland K, Pettersen S, Garman-Vik SS, Emilsen E, Nesland JM, Fodstad O and Engebraaten O: Modulation of glioma cell invasion and motility by adenoviral gene transfer of PAI-1. Clin Exp Metastasis 20: 301-309, 2003.
27. Humbert L and Lebrun JJ: TGF-beta inhibits human cutaneous melanoma cell migration and invasion through regulation of the plasminogen activator system. Cell Signal 25: 490-500, 2013.
28. Soff GA, Sanderowitz J, Gately S, Verrusio E, Weiss I, Brem S and Kwaan HC: Expression of plasminogen activator inhibitor type 1 by human prostate carcinoma cells inhibits primary tumor growth, tumor-associated angiogenesis, and metastasis to lung and liver in an athymic mouse model. J Clin Invest 96: 2593-2600, 1995.
29. Freeberg MAT, Farhat YM, Easa A, Kallenbach JG, Malcolm DW, Buckley MR, Benoit DSW and Awad HA: Serpine1 knockdown enhances MMP activity after flexor tendon injury in mice: Implications for adhesions therapy. Sci Rep 8: 5810, 2018.
30. Tang Z, Kang B, Li C, Chen T and Zhang Z: GEPIA2: An enhanced web server for large-scale expression profiling and interactive analysis. Nucleic Acids Res 47: W556-W560, 2019.
31. Yuan H, Yan M, Zhang G, Liu W, Deng C, Liao G, Xu L, Luo T, Yan H, Long Z, *et al*: CancerSEA: A cancer single-cell state atlas. Nucleic Acids Res 47: D900-D908, 2019.
32. Kanehisa M, Furumichi M, Sato Y, Matsuura Y and Ishiguro-Watanabe M: KEGG: Biological systems database as a model of the real world. Nucleic Acids Res 53: D672-D677, 2025.
33. Jura J: Animal models for the treatment of human diseases. Ann Anim Sci 24: 1153-1159, 2024.
34. Zhou YF, Wang QX, Zhou HY and Chen G: Autophagy activation prevents sevoflurane-induced neurotoxicity in H4 human neuroglioma cells. Acta Pharmacol Sin 37: 580-588, 2016.
35. Sun Y, Zhang Y, Cheng B, Dong Y, Pan C, Li T and Xie Z: Glucose may attenuate isoflurane-induced caspase-3 activation in H4 human neuroglioma cells. Anesth Analg 119: 1373-1380, 2014.
36. Yu X, Ambrosini G, Roszik J, Eterovic AK, Stempke-Hale K, Seftor EA, Chattopadhyay C, Grimm E, Carvajal RD, Hendrix MJ, *et al*: Genetic analysis of the 'uveal melanoma' C918 cell line reveals atypical BRAF and common KRAS mutations and single tandem repeat profile identical to the cutaneous melanoma C8161 cell line. Pigment Cell Melanoma Res 28: 357-359, 2015.
37. Bochman ML and Schwacha A: The Mcm complex: Unwinding the mechanism of a replicative helicase. Microbiol Mol Biol Rev 73: 652-683, 2009.
38. Lin DI, Aggarwal P and Diehl JA: Phosphorylation of MCM3 on Ser-112 regulates its incorporation into the MCM2-7 complex. Proc Natl Acad Sci USA 105: 8079-8084, 2008.
39. Aguirre-Ghiso JA, Estrada Y, Liu D and Ossowski L: ERK(MAPK) activity as a determinant of tumor growth and dormancy; regulation by p38(SAPK). Cancer Res 63: 1684-1695, 2003.
40. Aguirre-Ghiso JA, Liu D, Mignatti A, Kovalski K and Ossowski L: Urokinase receptor and fibronectin regulate the ERK(MAPK) to p38(MAPK) activity ratios that determine carcinoma cell proliferation or dormancy in vivo. Mol Biol Cell 12: 863-879, 2001.
41. Guereno M, Pastore MD, Lugones AC, Cercato M, Todaro L, Urtreger A and Peters MG: Glypican-3 (GPC3) inhibits metastasis development promoting dormancy in breast cancer cells by p38 MAPK pathway activation. Eur J Cell Biol 99: 151096, 2020.
42. Revathidevi S and Munirajan AK: Akt in cancer: Mediator and more. Semin Cancer Biol 59: 80-91, 2019.
43. Wu Q, Wu W, Fu B, Shi L, Wang X and Kuca K: JNK signaling in cancer cell survival. Med Res Rev 39: 2082-2104, 2019.
44. Xue A, Xue M, Jackson C and Smith RC: Suppression of urokinase plasminogen activator receptor inhibits proliferation and migration of pancreatic adenocarcinoma cells via regulation of ERK/p38 signaling. Int J Biochem Cell Biol 41: 1731-1738, 2009.
45. Wang C, Wu L, Bulek K, Martin BN, Zepp JA, Kang Z, Liu C, Herjan T, Misra S, Carman JA, *et al*: The psoriasis-associated D10N variant of the adaptor Act1 with impaired regulation by the molecular chaperone hsp90. Nat Immunol 14: 72-81, 2013.
46. Huangfu L, Li R, Huang Y and Wang S: The IL-17 family in diseases: From bench to bedside. Signal Transduct Target Ther 8: 402, 2023.
47. Lee YC, Yu CC, Lan C, Lee CH, Lee HT, Kuo YL, Wang PH and Chang WW: Plasminogen activator inhibitor-1 as regulator of tumor-initiating cell properties in head and neck cancers. Head Neck 38 (Suppl 1): E895-E904, 2016.
48. Nagase H, Visse R and Murphy G: Structure and function of matrix metalloproteinases and TIMPs. Cardiovasc Res 69: 562-573, 2006.
49. Cortez DM, Feldman MD, Mummidi S, Valente AJ, Steffensen B, Vincenti M, Barnes JL and Chandrasekar B: IL-17 stimulates MMP-1 expression in primary human cardiac fibroblasts via p38 MAPK- and ERK1/2-dependent C/EBP-beta , NF-kappaB, and AP-1 activation. Am J Physiol Heart Circ Physiol 293: H3356-H3365, 2007.
50. Feng W, Li W, Liu W, Wang F, Li Y and Yan W: IL-17 induces myocardial fibrosis and enhances RANKL/OPG and MMP/TIMP signaling in isoproterenol-induced heart failure. Exp Mol Pathol 87: 212-218, 2009.
51. Rana T, Jiang C, Banerjee S, Yi N, Zmijewski JW, Liu G and Liu RM: PAI-1 regulation of p53 expression and senescence in type II alveolar epithelial cells. Cells 12: 2008, 2023.
52. Samarakoon R and Higgins PJ: Integration of non-SMAD and SMAD signaling in TGF-beta1-induced plasminogen activator inhibitor type-1 gene expression in vascular smooth muscle cells. Thromb Haemost 100: 976-983, 2008.
53. Yang CH, Li HC, Ku TS, Wu PC, Yeh YJ, Cheng JC, Lin TY and Lo SY: Hepatitis C virus down-regulates SERPINE1/PAI-1 expression to facilitate its replication. J Gen Virol 98: 2274-2286, 2017.
54. Nepon-Sixt BS and Alexandrow MG: TGFbeta1 cell cycle arrest is mediated by inhibition of MCM assembly in Rb-deficient conditions. Mol Cancer Res 17: 277-288, 2019.
55. Czekay RP, Wilkins-Port CE, Higgins SP, Freytag J, Overstreet JM, Klein RM, Higgins CE, Samarakoon R and Higgins PJ: PAI-1: An integrator of cell signaling and migration. Int J Cell Biol 2011: 562481, 2011.
56. Lin Z, Huang Q, Liu J, Wang H, Zhang X, Zhu Z, Zhang W, Wei Y, Liu Z and Du W: Interleukin-17D promotes lung cancer progression by inducing tumor-associated macrophage infiltration via the p38 MAPK signaling pathway. Aging (Albany NY) 14: 6149-6168, 2022.
57. Xiang T, Long H, He L, Han X, Lin K, Liang Z, Zhuo W, Xie R and Zhu B: Interleukin-17 produced by tumor microenvironment promotes self-renewal of CD133+ cancer stem-like cells in ovarian cancer. Oncogene 34: 165-176, 2015.
58. Li X, Bechara R, Zhao J, McGeachy MJ and Gaffen SL: IL-17 receptor-based signaling and implications for disease. Nat Immunol 20: 1594-1602, 2019.
59. Zhang X, Li B, Lan T, Chiari C, Ye X, Wang K and Chen J: The role of interleukin-17 in inflammation-related cancers. Front Immunol 15: 1479505, 2024.
60. Tomcik M, Zerr P, Pitkowski J, Palumbo-Zerr K, Avouac J, Distler O, Becvar R, Senolt L, Schett G and Distler JH: Heat shock protein 90 (Hsp90) inhibition targets canonical TGF-β signalling to prevent fibrosis. Ann Rheum Dis 73: 1215-1222, 2014.
61. Korabiowska M, Betke H, Brinck U, Grohmann U, Hönig JF and Droese M: Loss of growth arrest DNA damage genes expression in oral melanomas. In Vivo 13: 483-485, 1999.
62. Schneider DJ, Chen Y and Sobel BE: The effect of plasminogen activator inhibitor type 1 on apoptosis. Thromb Haemost 100: 1037-1040, 2008.

63. Zhang YP, Wang WL, Liu J, Li WB, Bai LL, Yuan YD and Song SX: Plasminogen activator inhibitor-1 promotes the proliferation and inhibits the apoptosis of pulmonary fibroblasts by Ca(2+) signaling. Thromb Res 131: 64-71, 2013.
64. Bajou K, Peng H, Laug WE, Maillard C, Noel A, Foidart JM, Martial JA and DeClerck YA: Plasminogen activator inhibitor-1 protects endothelial cells from FasL-mediated apoptosis. Cancer Cell 14: 324-334, 2008.
65. Zhao C and Liu Z: MicroRNA 617 Targeting SERPINE1 inhibited the progression of oral squamous cell carcinoma. Mol Cell Biol 41: e0056520, 2021.
66. Yahata T, Ibrahim AA, Hirano KI, Muguruma Y, Naka K, Hozumi K, Vaughan DE, Miyata T and Ando K: Targeting of plasminogen activator inhibitor-1 activity promotes elimination of chronic myeloid leukemia stem cells. Haematologica 106: 483-494, 2021.
67. Adeshakin FO, Adeshakin AO, Afolabi LO, Yan D, Zhang G and Wan X: Mechanisms for modulating anoikis resistance in cancer and the relevance of metabolic reprogramming. Front Oncol 11: 626577, 2021.
68. Weems AD, Welf ES, Driscoll MK, Zhou FY, Mazloom-Farsibaf H, Chang BJ, Murali VS, Gihana GM, Weiss BG, Chi J, *et al*: Blebs promote cell survival by assembling oncogenic signalling hubs. Nature 615: 517-525, 2023.
69. Yu XM, Jaskula-Sztul R, Georgen MR, Aburjania Z, Somnay YR, Leverson G, Sippel RS, Lloyd RV, Johnson BP and Chen H: Notch1 signaling regulates the aggressiveness of differentiated thyroid cancer and inhibits SERPINE1 expression. Clin Cancer Res 22: 3582-3592, 2016.
70. Kim WT, Mun JY, Baek SW, Kim MH, Yang GE, Jeong MS, Choi SY, Han JY, Kim MH and Leem SH: Secretory SERPINE1 expression is increased by antiplatelet therapy, inducing MMP1 expression and increasing colon cancer metastasis. Int J Mol Sci 23: 9596, 2022.
71. Wu Z, He D, Zhao S and Wang H: IL-17A/IL-17RA promotes invasion and activates MMP-2 and MMP-9 expression via p38 MAPK signaling pathway in non-small cell lung cancer. Mol Cell Biochem 455: 195-206, 2019.
72. Wu Y, Zhu L, Liu L, Zhang J and Peng B: Interleukin-17A stimulates migration of periodontal ligament fibroblasts via p38 MAPK/NF-kappaB -dependent MMP-1 expression. J Cell Physiol 229: 292-299, 2014.
73. Shibabaw T, Teferi B and Ayelign B: The role of Th-17 cells and IL-17 in the metastatic spread of breast cancer: As a means of prognosis and therapeutic target. Front Immunol 14: 1094823, 2023.
74. Nuha N, Higgins SP, Czekay RP, Higgins CE, Guo L, Lee H and Higgins PJ: SERPINE1 drives molecular synergies in colorectal cancer. Am J Physiol Cell Physiol 330: C9-C25, 2026.